crystals

MDPI

Article

Pre-Polymer Chain Length: Influence on Permanent Memory Effect of PDLC Devices

Ana Mouquinho, Maria Teresa Barros and João Sotomayor *

LAQV-REQUIMTE, Department of Chemistry, NOVA School of Science and Technology, NOVA University of Lisbon, 2829-516 Caparica, Portugal; a.mouquinho@campus.fct.unl.pt (A.M.); mtb@fct.unl.pt (M.T.B.)
* Correspondence: sotomayor@fct.unl.pt

Abstract: This study delved into the correlation between the chain length of PEG polymerizable oligomers and the electro-optical properties exhibited by the resultant PDLC films. A range of di(meth)acrylate oligomers derived from polyethylene glycol with varying molecular weights (Mn = 1000, 2000, 4000, and 6000 g mol^{-1}) was synthesized for incorporation as the polymer matrix in PDLC devices. Comprehensive analyses employing ^{1}H-NMR, ^{13}C-NMR, and MALDI-TOF mass spectroscopy were conducted to validate the structure and purity of the synthesized products. The investigation revealed a significant influence of pre-polymer molecular chain length on the thermal properties of the polymer, including amorphousness and crystallinity, which in turn impact the permanent memory effect. Specifically, it was observed that amorphous PEG polymers serve as an ideal matrix for fostering the permanent memory effect in PDLCs. Among the polymerizable PEG oligomers examined, those with a molecular weight of 1000 g/mol yielded polymer chains existing in an amorphous state, exhibiting a glass transition temperature lower than room temperature (−50 °C). This characteristic imparts flexibility and mobility to the polymer matrix chains, facilitating a 37% permanent memory effect. Conversely, longer polymer chains lead to the formation of crystal aggregates, resulting in semi-crystalline polymer matrices. This reduces the malleability of the polymer chains, thereby nullifying the permanent memory effect in the corresponding PDLC devices.

Keywords: polymer-dispersed liquid crystals; memory devices; permanent memory effect; liquid crystals

Citation: Mouquinho, A.; Barros, M.T.; Sotomayor, J. Pre-Polymer Chain Length: Influence on Permanent Memory Effect of PDLC Devices. *Crystals* **2024**, *14*, 249. https://doi.org/10.3390/cryst14030249

Academic Editor: Francesco Simoni

Received: 30 January 2024
Revised: 21 February 2024
Accepted: 26 February 2024
Published: 2 March 2024

1. Introduction

Electro-optical effects in polymer-dispersed liquid crystal (PDLC) films occur through the manipulation of the configuration of liquid-crystal (LC) molecules within LC domains under the influence of an electric field. However, the polymer matrix not only provides mechanical support for the LC domains but also, depending on its thermal properties, can lead to the emergence of two distinct long-lived states with varying optical properties, such as opacity or transparency, when the electric field is switched off.

When the glass transition temperature (Tg) of the polymer matrix exceeds room temperature or when it is composed of a crystalline polymer (as illustrated in Figure 1a), a scattering state is observed. Conversely, a highly transparent state can be maintained when the Tg of the polymer matrix is lower than room temperature (as depicted in Figure 1b).

Polymers can exist in either an amorphous or crystalline state. Crystalline polymers exhibit a well-defined chain conformation, forming a structured arrangement, unlike amorphous polymers which feature a disordered structure akin to a tangled mass of chains, resembling a bowl of spaghetti [2,3]. However, it is worth noting that even in crystalline polymers, there can be local amorphous regions, albeit with some vague and localized order [4].

When amorphous polymers are adequately cooled, they can resemble glass. Above this glassy state, segmental mobility is not zero, allowing for short-range vibrational and

rotational motions of the polymer segments. This segmental motion grants the polymer some level of ductility. At temperatures surpassing the glassy state, larger molecule motion resumes, and if the amorphous polymer is crosslinked, it behaves like rubber. Without crosslinking, amorphous polymers exhibit properties akin to highly viscous liquids.

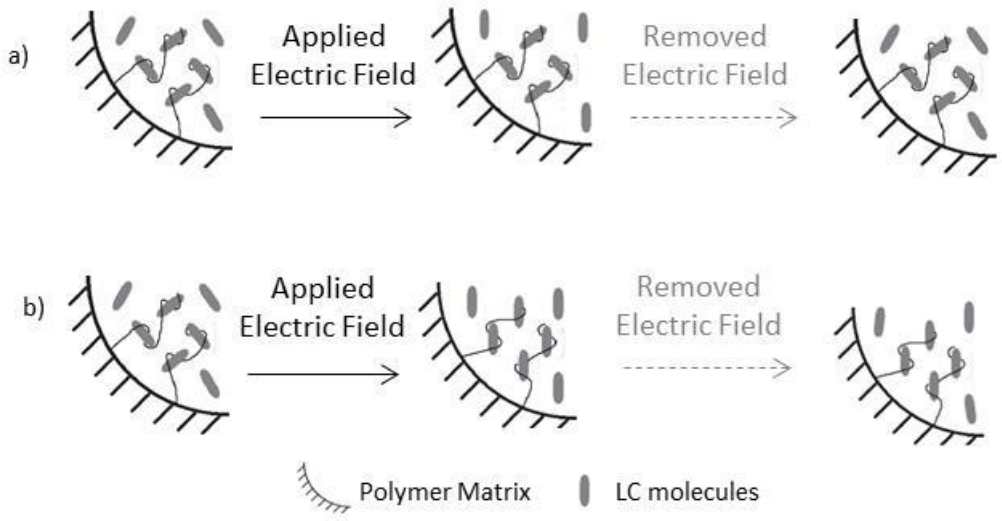

Figure 1. A simplified illustration of liquid-crystal orientation influenced by thermal properties of the polymer: (**a**) Tg higher than room temperature or crystalline polymer and (**b**) Tg lower than room temperature (adapted from [1]).

This pivotal transition point is termed the glass transition, denoted as Tg. The precise value of Tg is heavily reliant on various factors, including the attractive forces between chains, the repeating unit, the molecular architecture, the number of functionalities, and the molecular weight [4].

In general, the reduction in molecular weight of oligomers for linear chains intensifies the attractive forces between chains, consequently demanding more thermal energy to transition from a glassy to a rubbery state. Consequently, the Tg values of corresponding polymers tend to increase as the molecular weight of the oligomer decreases [4,5]. Conversely, when there is a significant increase in molecular chain length, highly entangled long chains in the melt can give rise to a crystalline state [6–8]. The inherently long-chain nature of macromolecules results in a crystallization mechanism and crystal morphology that starkly differs from those of small molecules [9], leading to a pronounced contrast in the crystallization process between low molecular weight and macromolecular systems [10].

The polymer chain length, whether short or long, typically yields randomly coiled and entangled chains, imparting amorphous characteristics [5]. In contrast, small molecules readily allow for the transportation and independent rearrangement of each atom or molecule into crystalline points during phase transition from a liquid to a crystal. This mechanism involves nucleation followed by growth stages. However, in macromolecular systems, the transportation and rearrangement of each polymer chain molecule are considerably hindered due to entanglement in longer polymer chains. Consequently, the chains must slide along their axes to facilitate rearrangement into a crystalline phase [10]. Despite chain folding predominantly driving the crystallization process, many chains remain in a disordered structure, resulting in a semi-crystalline morphology [6].

The semi-crystalline arrangement of macromolecules manifests as chains traversing several fibrillary crystallites via intermediate amorphous regions. Notably, the same chain may alternate between ordered and disordered regions [11]. (Refer to Figure 2 for visual representation).

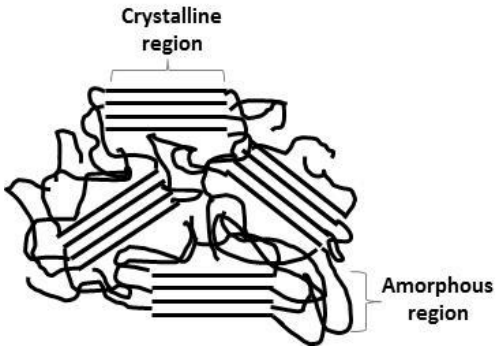

Figure 2. Schematic illustration of fringed-micelle model of the microstructure of semi-crystalline macromolecules (adapted from [11]).

When crystallization occurs from concentrated or molten solutions, it leads to the formation of multilamellar aggregates. The prevailing structure typically comprises radiating arrays of period lamellae stemming from a core, interconnected by amorphous regions, with crystal aggregates typically adopting a circular crystalline shape known as spherulites [12].

The development of folded-chain crystal morphologies necessitates a critical molecular weight for chains to initiate folding. If the molecular weight exceeds this critical threshold, folded-chain crystals may form. A minimum chain length is required to initiate crystallite formation; in other words, the molecular chain must be sufficiently long to facilitate both folding and crystallization [13,14]. In highly crystalline polymers, the small amorphous component experiences significant confinement due to the presence of crystals. Molecular chains shorter than the critical length are incapable of participating in chain-fold crystallization and are thereby excluded [11]. Typically, molecular chains below the critical molecular weight can only interlink, akin to cooked spaghetti, resulting in the formation of amorphous regions [15].

However, despite the necessity for a minimum chain length, the level of crystallinity decreases significantly with a considerable increase in molar mass. As mentioned earlier, nucleation involves the disentanglement of molecular chains to facilitate rearrangement into folded conformations. This nucleation process becomes increasingly challenging with rising molecular weight due to heightened friction impeding sliding diffusion [10]. With increasing molar mass, the freedom of chains to rearrange themselves during crystallization diminishes, resulting in less regular chain folding [11]. Consequently, at higher molar masses, a larger proportion of the sample crystallizes with chains remaining in the amorphous phase. Some of these chains in the amorphous region may re-enter the same crystal lamella after a stint in the amorphous phase [4].

2. Materials and Methods

The nematic liquid-crystalline mixture E7, purchased from Merck, is a eutectic blend characterized by a positive dielectric anisotropy at T = 20 °C (with an ordinary refractive index, no = 1.5183, and an extraordinary refractive index, ne = 1.7378, both at 20 °C) and a nematic–isotropic transition temperature of T_{NI} = 58 °C. It comprises 4-cyano-4′-pentyl-1,1′-biphenyl (51%), 4-n-heptyl-4′-cyanobiphenyl (25%), 4,4′-n-octyloxycyanobiphenyl (16%), and 4′-n-pentyl-4-cyanotriphenyl (8%) *w*/*w* [16].

The initiator for thermal polymerization, 2,2′-azobis(isobutyronitrile) (AIBN), was procured from Aldrich and used as received. Methacryloyl chloride and acryloyl chloride, also sourced from Aldrich, were utilized without further purification. PEGs obtained from Aldrich were subjected to vacuum drying over P_2O_5 to eliminate residual water content. Additionally, the solvents and triethylamine from Aldrich underwent purification prior to use. Column chromatography was conducted using silica gel from Macherey-Nagel (Kieselgel 60 M). Reaction progress was monitored via thin-layer chromatography (TLC)

performed on aluminum-backed silica gel Merck 60 F254 plates. Compound visualization was facilitated using UV light (254 nm) and/or staining with a solution of phosphomolybdic acid (5 g) in EtOH (95 mL) followed by heating. All reactions were carried out under a dry argon atmosphere.

Mass spectra were obtained using matrix-assisted laser desorption ionization time-of-flight (MALDI-TOF) on a Bruker Autoflex instrument. The matrix employed was 2-(4-hydroxyphenylazo)benzoic acid (HABA), with sodium cationization. NMR spectra were acquired using a Bruker AMx-400 MHz spectrometer, operating at 400 MHz for ^{1}H nuclei and 100 MHz for ^{13}C nuclei. Deuterated chloroform ($CDCl_3$) with 99.50% isotopic purity, sourced from Aldrich, was utilized as the solvent, with chemical shift values (δ) reported in parts per million (ppm) relative to tetramethylsilane (TMS), serving as the internal reference.).

2.1. Preparation of PDLC

The PDLCs were fabricated by blending a homogeneous solution comprising 70 wt.% (weight percentage) of LC E7, 30 wt.% of pre-polymer, with 1 wt.% of the thermal initiator, N,N-azobisisobutyronitrile (AIBN). This mixture was filled into a commercial electro-optical cell, LC2-20.0 supplied by Instec Inc, with a 20 μm spacer between indium tin oxide (ITO) substrates, facilitated by capillary action. The LC2-20.0 electro-optical cells are 15.25x17 mm transparent cells with an ITO area of 5x5 mm, where an electric field can be applied between de two conducting glasses of the cell, separated by the 20 μm spacer.

The thermal properties of the polymer were assessed using differential scanning calorimetry DSC Q2000 model from TA Instruments, interfaced with a cooling accessory. Measurements were conducted under a nitrogen atmosphere with a flow rate of approximately 50 mL/min. Samples weighing around 2 mg were encapsulated in hermetically sealed aluminum pans (6 mm base diameter, 4.2 mm deep), with an empty pan serving as the reference. Thermal properties were evaluated through various cooling/heating cycles spanning from −80 °C to 130 °C, employing a cooling/heating rate of 5 °C/min to ascertain the reversibility of thermal transitions.

Evaluation of liquid-crystal domains was performed using a polarizing optical microscope (POM). This method also facilitated the examination of the effect of electric fields on the configuration and orientation of LC domains. Experiments were conducted using an Olympus CX31P optical polarizing microscope connected to an Olympus SC-30 digital camera interfaced with a computer. Microphotographs depicting the dispersion of liquid-crystal domains in PDLC films were captured at a magnification of 100× under crossed polarizers.

For thermal polymerizations, a custom-made oven equipped with an auto-tune temperature controller (CAL Controls, model CAL 3300) and a resistance thermometer (Pt100/RTD-2) was employed. The resistance thermometer sensor offered a temperature range spanning from −200 to 400 °C.

2.2. Electro-Optical Characterization

For the electro-optical characterization of PDLC films, transmittance measurements were conducted while progressively increasing and then decreasing the voltage. Light transmittance studies were carried out using a diode array Avantes spectrophotometer (The Netherlands) (AvaLight-DHS and AvaSpec 2048, Avantes, Apeldoorn, The Netherlands) equipped with a halogen lamp and optical fiber connections. A wavelength of 633 nm was chosen for the analysis. An electric pulse at a frequency of 1 kHz was generated using a programmable waveform generator (Wavetek 20 MHz Synthesized Function Generator Model 90, Wavetek, Hsinchu County, Taiwan), producing an alternating current (AC) wave with a low amplitude ranging between 0 and 27 VRMS for sample excitation.

For the electro-optical measurements, an external electric field was applied across the PDLC film. The generator, connected to a Vtrek TP-430 amplifier, delivered a voltage of 47 VRMS, which was then amplified by a factor of 24 using a 220 V/9 V transformer

connected in reverse. A 1 Ω resistance was employed to protect the amplifier from short-circuits, while a 150 kΩ resistance was utilized to standardize the voltage wave output. The amplifier was powered by a Kiotto KPS 1310 power supply. The output detector (AvaSpec-2048) was linked to computer software for data acquisition.

3. Results

3.1. Synthesis, NMR, and MALDI-TOF Characterization of Poly(ethylene glycol) End-Functionalized

3.1.1. Poly(ethylene glycol) Dimethacrylate, PEG2000DM

In a typical synthesis, poly(ethylene glycol) (Mw = 2000 g mol^{-1}) (2 g, 1 mmol, 1 eq) was dissolved in dry CH_2Cl_2 (15 mL), followed by the addition of triethylamine (0.4 g, 4 mmol, 4 eq). The solution was then cooled to 0 °C in an ice-water bath. Methacryloyl chloride (0.42 g, 4 mmol, 4 eq) was added dropwise to the cooled solution. After complete addition, the mixture was stirred for 24 h at 40 °C.

The reaction mixture was subsequently washed with 0.1 M HCl, brine, and water. Any residual water in the organic phase was removed by treatment with anhydrous Na_2SO_4, followed by filtration and concentration under reduced pressure. The resulting solution was then added dropwise to 300 mL of diethyl ether, which had been cooled on an ice bath. The product was collected by filtration and washed with diethyl ether. TLC analysis using $CHCl_3$-MeOH (9:1) as the mobile phase confirmed the formation of the desired product.

A white waxy solid (1.67 g, 0.78 mmol, 78% yield) was obtained after purification.

The NMR assignments and structure determination were conducted using ^{1}H-NMR (Figure 3) and ^{13}C-NMR (Figure 4).

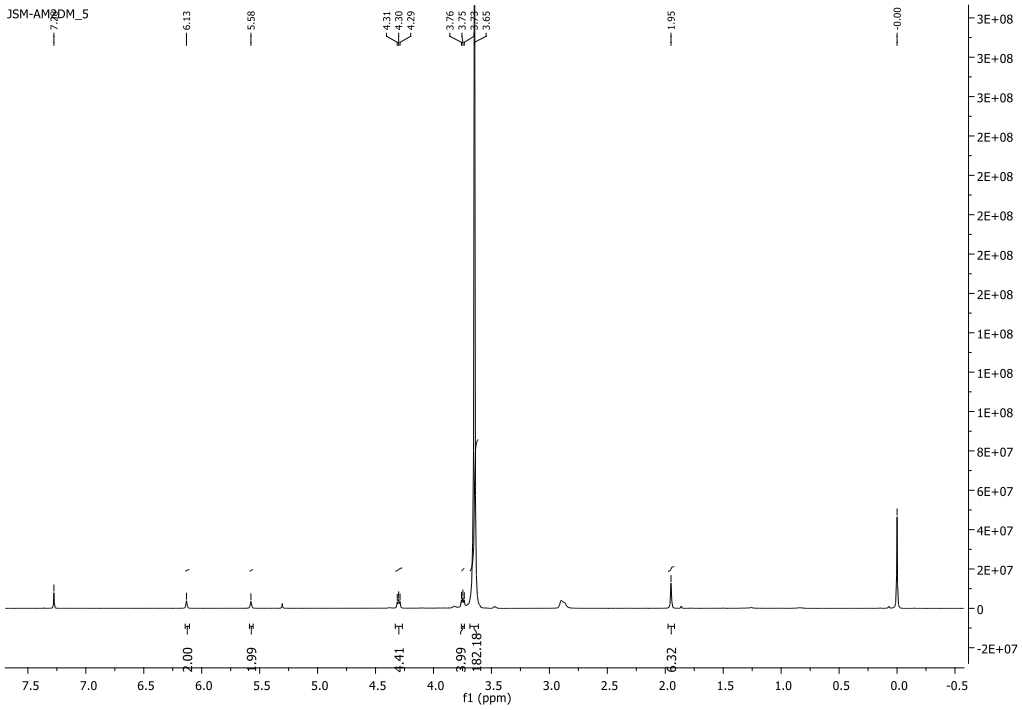

Figure 3. ^{1}H-NMR spectrum of PEG2000DM.

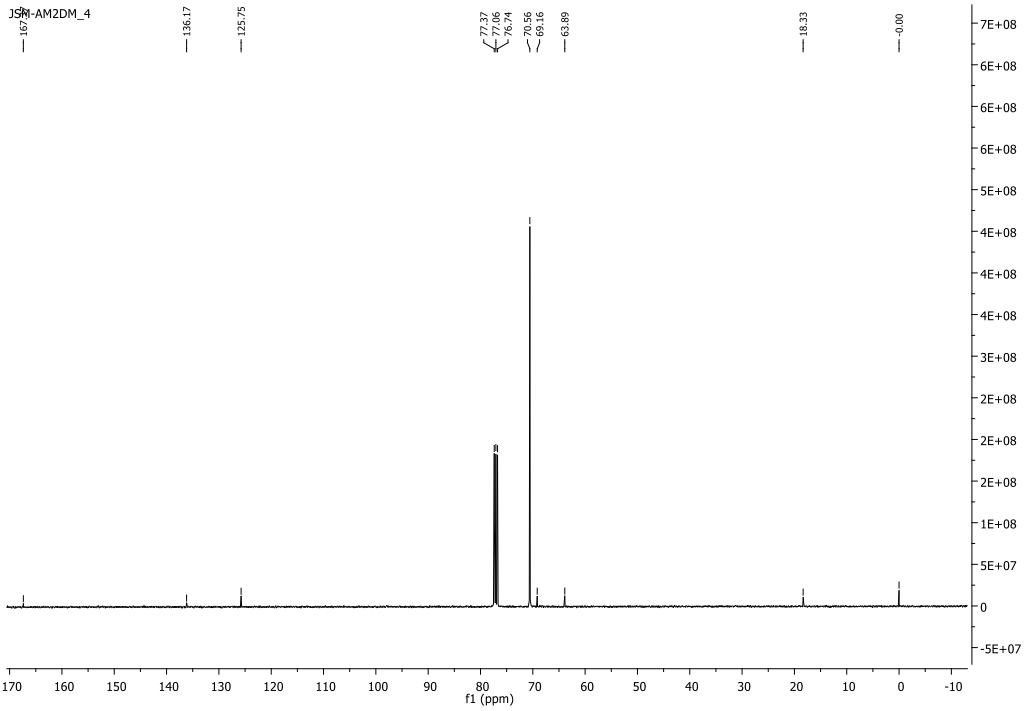

Figure 4. ^{13}C-NMR spectrum of PEG2000DM.

^{1}H-NMR (400 MHz, $CDCl_3$) δ 6.13 (s, 2H, =C$\underline{H_2}$), 5.58 (s, 2H, =C$\underline{H_2}$), 4.32–4.28 (m, 4H, C$\underline{H_2}$O-(C=O)), 3.76–3.72 (m, 4H, C$\underline{H_2}$CH$_2$O-(C=O)), 3.65 (s, 182H, C$\underline{H_2}$C$\underline{H_2}$O), 1.95 (s, 6H, C$\underline{H_3}$).
^{13}C-NMR (100 MHz, $CDCl_3$) δ 18.13 (C$\underline{H_3}$), 63.99 (C$\underline{H_2}$O-(C=O)), 69.16 (C$\underline{H_2}$CH$_2$O-(C=O)), 70.56 (C$\underline{H_2}$C$\underline{H_2}$O), 125.75(=C$\underline{H_2}$), 136.17(H$_3$C-C$\underline{=}$), 167.33 (C$\underline{=}$O).

3.1.2. Poly(ethylene glycol) Dimethacrylate, PEG4000DM and PEG6000DM

The synthesis and characterization of PEG4000DM and PEG6000DM followed a similar protocol to that of PEG2000DMA, with the substitution of PEG2000 for PEG4000 and PEG6000, respectively.

For PEG4000DM synthesis, poly(ethylene glycol) (Mw = 4000 g mol^{-1}) (2 g, 0.5 mmol, 1 eq) was dissolved in CH_2Cl_2 (15 mL), followed by the addition of triethylamine (0.2 g, 2 mmol, 4 eq) and methacryloyl chloride (0.21 g, 2 mmol, 4 eq). The reaction yielded PEG4000DM (1.63 g, 0.39 mmol, 79% yield) as a white waxy solid that foamed under vacuum.

The NMR assignments and structure determination were conducted using ^{1}H-NMR (Figure 5) and ^{13}C-NMR (Figure 6).

^{1}H-NMR (400 MHz, $CDCl_3$) δ 6.13 (s, 2H, =C$\underline{H_2}$), 5.57 (s, 2H, =C$\underline{H_2}$), 4.31–4.28 (m, 4H, C$\underline{H_2}$O-(C=O))3.76–3.73 (m, 4H, C$\underline{H_2}$CH$_2$O-(C=O)),3.65 (s, 69H, C$\underline{H_2}$C$\underline{H_2}$O),1.95 (s, 6H, C$\underline{H_3}$).
^{13}C-NMR (100 MHz,$CDCl_3$) δ 18.33 (C$\underline{H_3}$), 63.879 (C$\underline{H_2}$O-(C=O)), 69.16 (C$\underline{H_2}$CH$_2$O-(C=O)), 70.58 (C$\underline{H_2}$C$\underline{H_2}$O), 125.75(=C$\underline{H_2}$), 136.18(H$_3$C-C$\underline{=}$), 167.37 (C$\underline{=}$O).

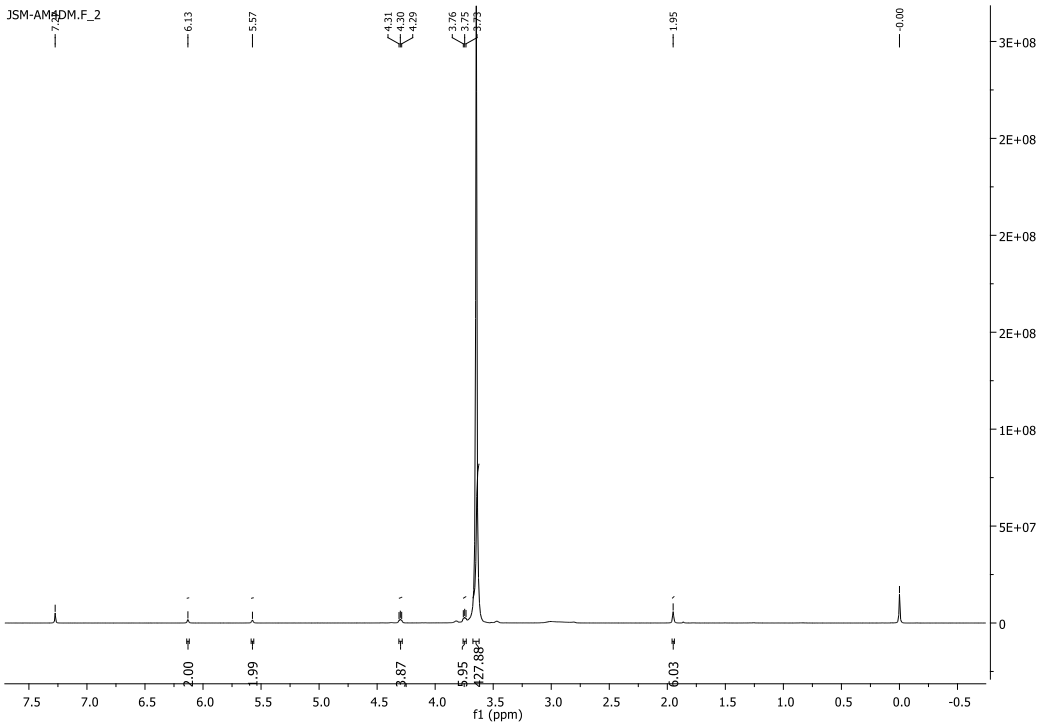

Figure 5. ^{1}H-NMR spectrum of PEG4000DM.

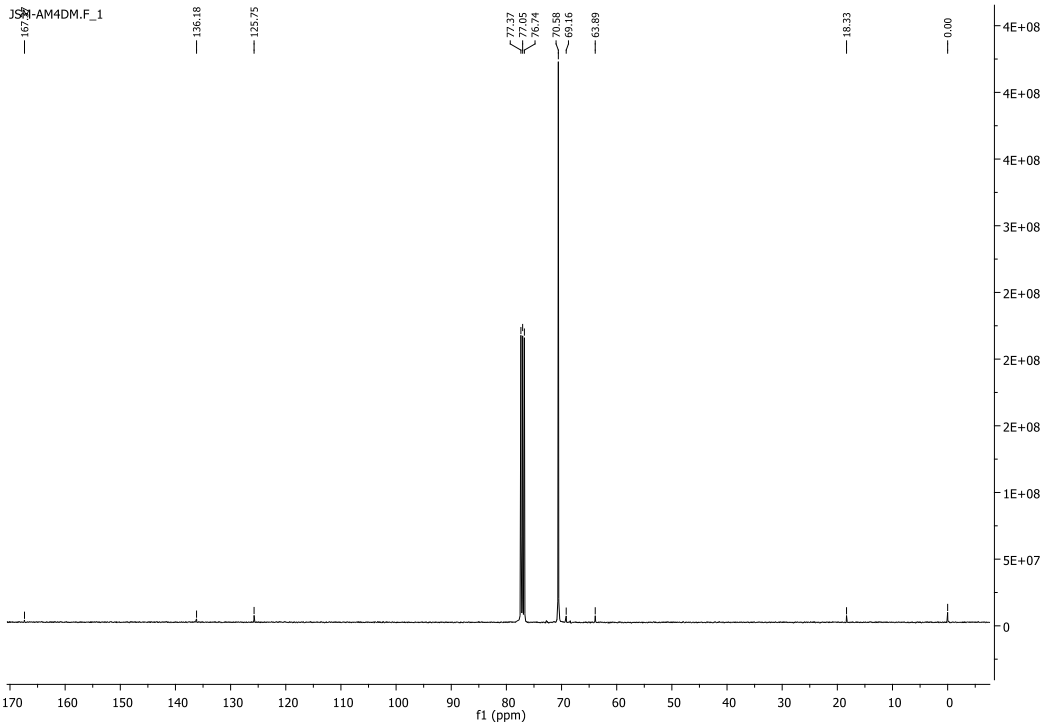

Figure 6. ^{13}C-NMR spectrum of PEG4000DM.

Poly(ethylene glycol) (Mw = 6000 g mol^{-1}) (2 g, 0.33 mmol, 1 eq) was dissolved in CH_2Cl_2 (15 mL) followed by the addition of triethylamine (0.14 g, 1.33 mmol, 4 eq) and methacryloyl chloride (0.14 g, 1.33 mmol, 4 eq). The reaction yielded PEG6000DM (1.69 g, 0.28 mmol, 82 %) as a white waxy solid that foamed under vacuum.

The NMR assignments and structure determination were conducted using ^{1}H-NMR (Figure 7) and ^{13}C-NMR (Figure 8).

^{1}H-NMR (400 MHz, $CDCl_3$) δ 6.12 (s, 2H, =C$\underline{H}_2$), 5.57 (s, 2H, =C$\underline{H}_2$), 4.31–4.28 (m, 4H, C$\underline{H}_2$O-(C=O)), 3.83–3.79 (m, 4H, C$\underline{H}_2$CH$_2$O-(C=O)), 3.64 (s, 525H, C$\underline{H}_2$C$\underline{H}_2$O), 1.94 (s, 6H, C$\underline{H}_3$).
^{13}C-NMR (100 MHz, $CDCl_3$) δ 18.36 (C$\underline{H}_3$), 63.92 (C$\underline{H}_2$O-(C=O)), 69.18 (C$\underline{H}_2$CH$_2$O-(C=O)), 70.61 (C$\underline{H}_2$C$\underline{H}_2$O), 125.77(=C$\underline{H}_2$), 136.20(H$_3$C-C$\underline{=}$), 167.39 (C$\underline{=}$O).

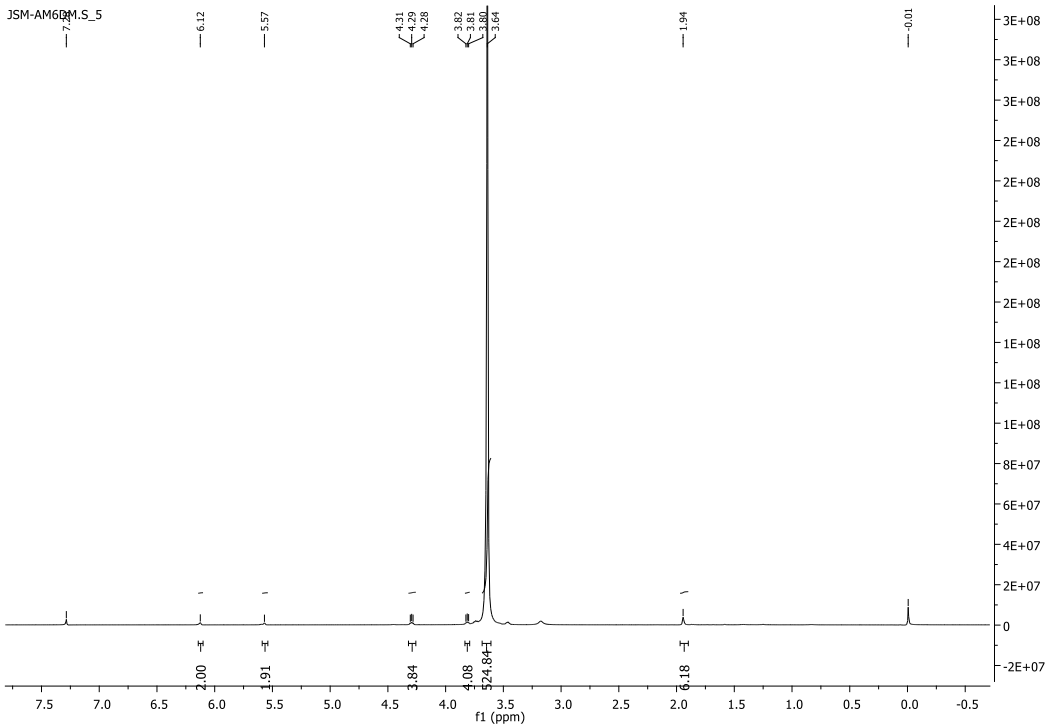

Figure 7. ^{1}H-NMR spectrum of PEG6000DM.

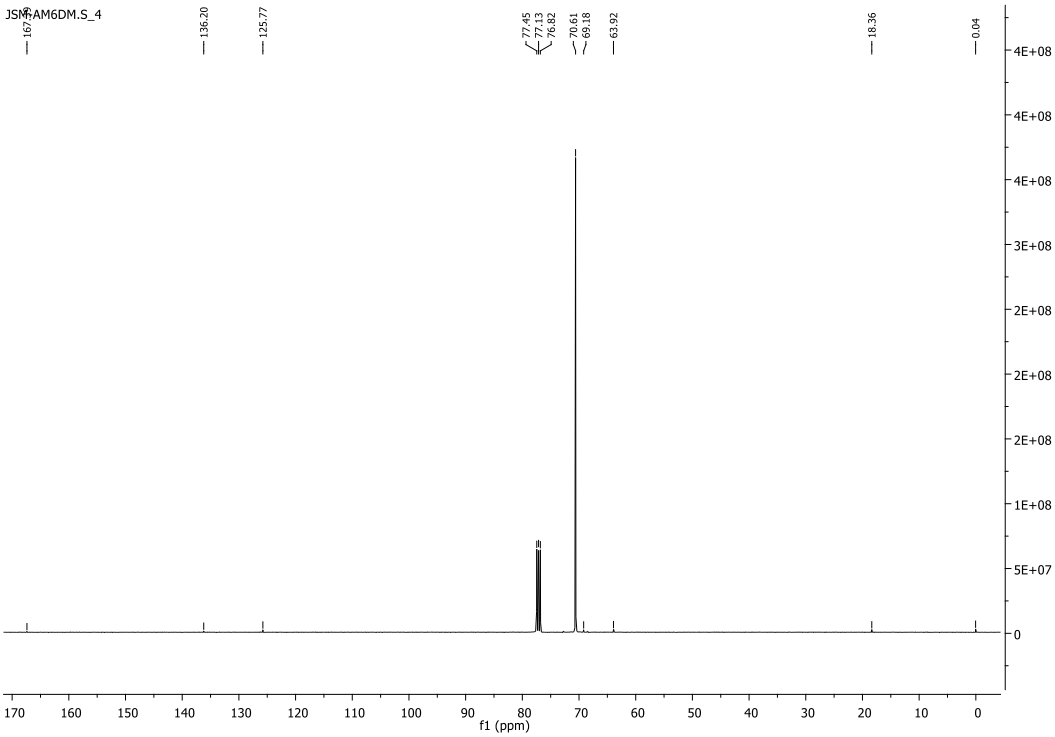

Figure 8. ^{13}C-NMR spectrum of PEG6000DM.

3.1.3. Poly(ethylene glycol) Dimethacrylate, PEG1000DM

The synthesis of PEG1000DM followed a similar procedure as described above, with the resulting crude product subsequently purified by column chromatography using EtOAC-hexane (5:1) followed by $CHCl_3$:MeOH (9:1). Compounds were visualized using phosphomolybdic acid by TLC analysis ($CHCl_3$-MeOH 9:1).

Poly(ethylene glycol) (Mw = 1000 g mol^{-1}) (2 g, 2 mmol, 1 eq) was dissolved in CH_2Cl_2 (15 mL), and then triethylamine (0.81 g, 8 mmol, 4 eq) and methacryloyl chloride (0.84 g, 8 mmol, 4 eq) were added. The reaction produced PEG1000DM (2.02 g, 1.78 mmol, 89% yield) as a colorless oil that foamed under vacuum.

The NMR assignments and structure determination were conducted using ^{1}H-NMR (Figure 9), ^{13}C-NMR (Figure 10), Dept (Figure 11), and using two-dimensional NMR (COSY (Figure 12) and HSQC (Figure 13)).

^{1}H-NMR (400 MHz, $CDCl_3$) δ 6.13 (s, 2H, =C$\underline{H_2}$), 5.58 (s, 2H, =C$\underline{H_2}$), 4.32–4.28 (m, 4H, C$\underline{H_2}$O-(C=O)), 3.77–3.72 (m, 4H, C$\underline{H_2}$C$\underline{H_2}$O-(C=O)), 3.65 (s, 69H, C$\underline{H_2}$C$\underline{H_2}$O), 1.95 (s, 6H, C$\underline{H_3}$).

^{13}C-NMR (100 MHz, $CDCl_3$) δ 18.31 (C$\underline{H_3}$), 63.87 (C$\underline{H_2}$O-(C=O)), 69.12 (C$\underline{H_2}$C$\underline{H_2}$O-(C=O)), 70.54 (C$\underline{H_2}$C$\underline{H_2}$O), 125.74(=C$\underline{H_2}$), 136.14(H$_3$C-C$\underline{=}$), 167.34 (C$\underline{=}$O).

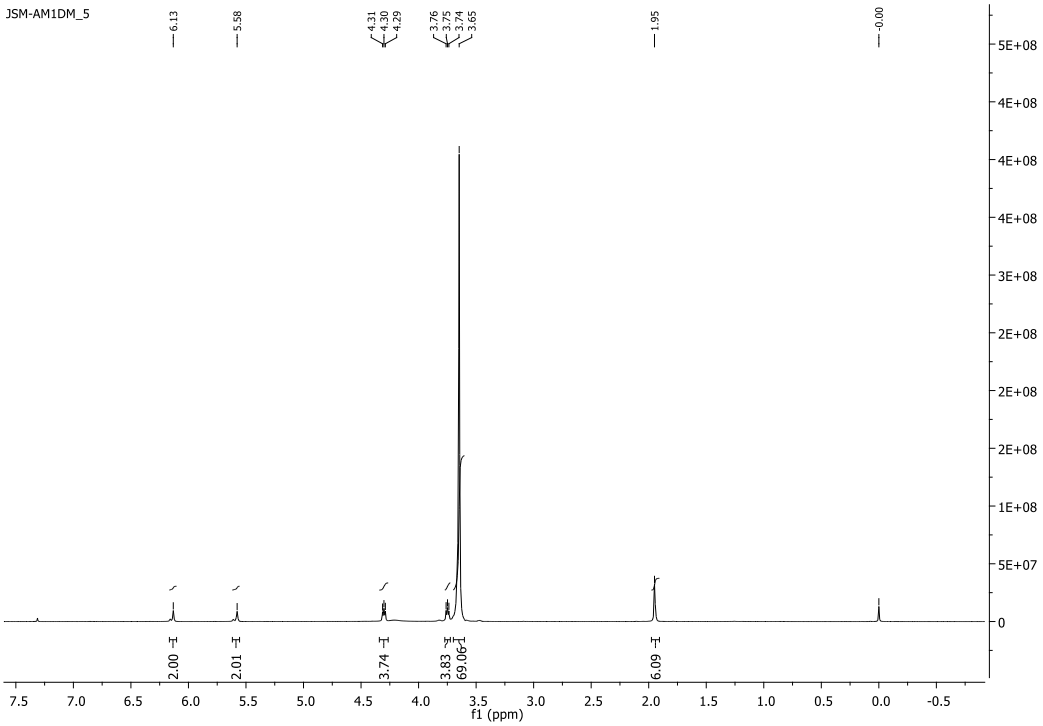

Figure 9. ^{1}H-NMR spectrum of PEG1000DM.

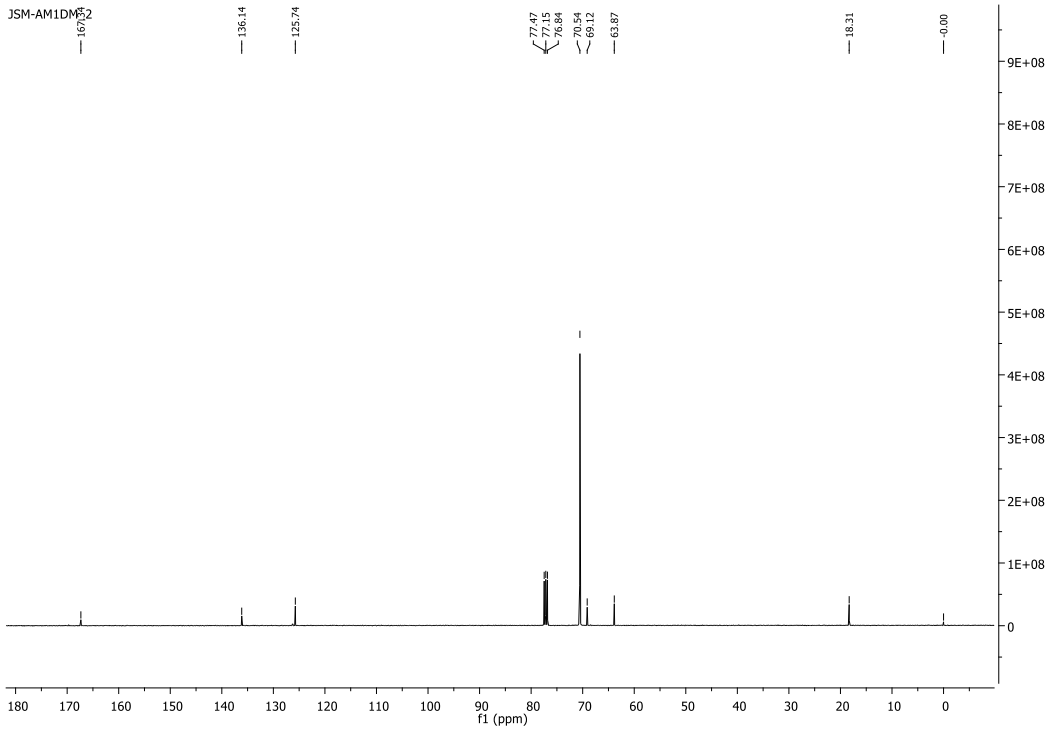

Figure 10. ^{13}C-NMR spectrum of PEG1000DM.

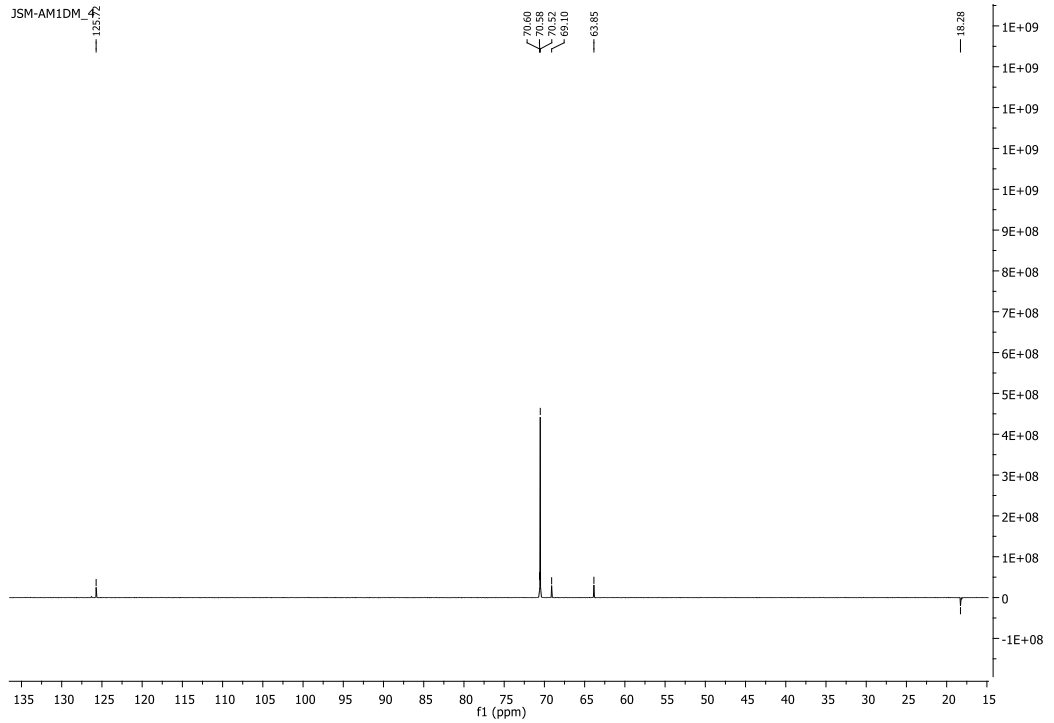

Figure 11. ^{13}C DEPT spectrum of PEG1000DM.

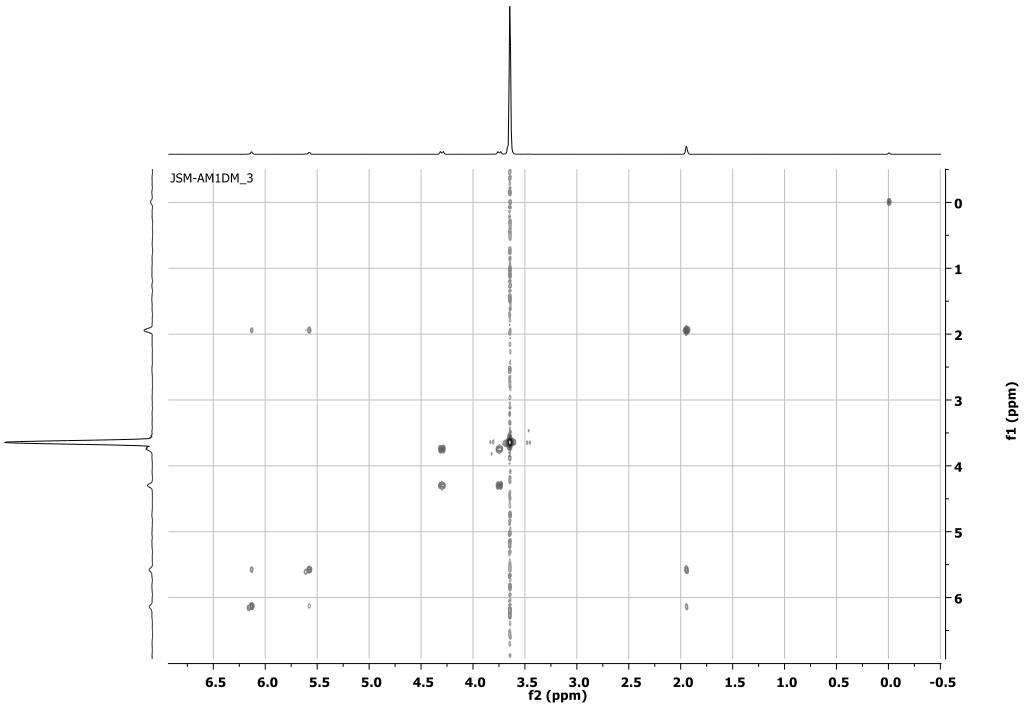

Figure 12. COSY spectrum of PEG1000DM.

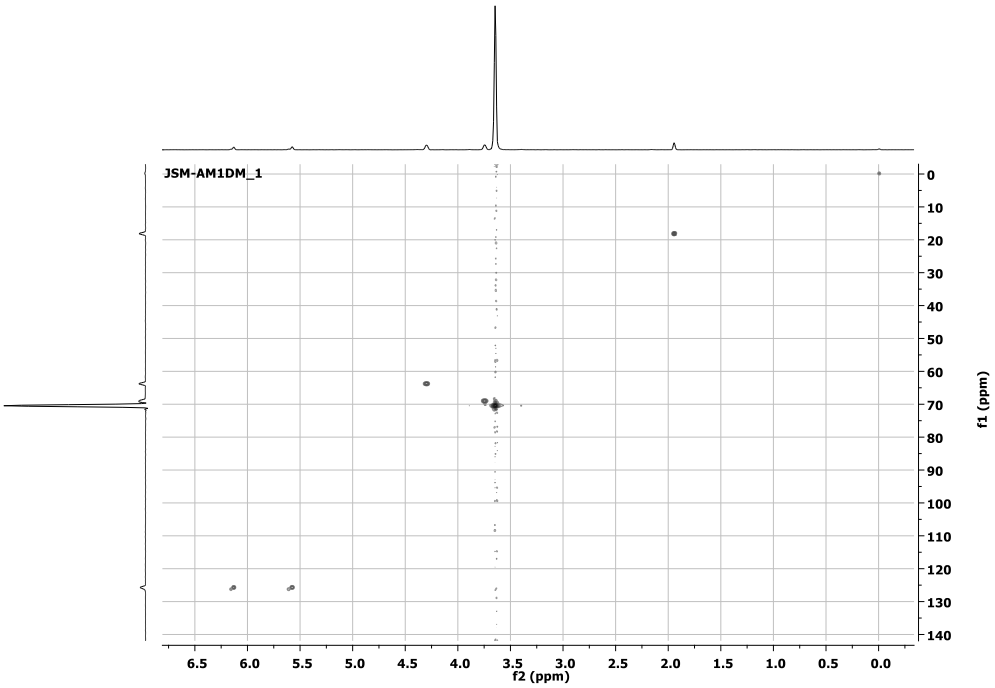

Figure 13. HSQC spectrum of PEG1000DM.

3.1.4. Poly(ethylene glycol) Diacrylate, PEG2000DA

Poly(ethylene glycol) (Mw = 2000 g mol^{-1}) (2 g, 1 mmol, 1 eq) was dissolved in CH_2Cl_2 (15 mL) and then triethylamine (0.41 g, 4 mmol, 4 eq) and acryloyl chloride (0.36 g, 4 mmol, 4 eq) were added. The reaction produced PEG2000DA (1.45 g, 0.69 mmol, 69% yield) as a white waxy solid that foamed under vacuum.

The NMR assignments and structure determination were conducted using ^{1}H-NMR (Figure 14) and ^{13}C-NMR (Figure 15).

^{1}H-NMR (400 MHz, $CDCl_3$) δ 6.16 (d, *J* = 17.3 Hz, 2H, =C$\underline{H}_2$), 6.16 (dd, *J* = 17.4, 10.4 Hz, 2H, =C$\underline{H}$), 5.84 (d, *J* = 10.4 Hz, 1H, =C$\underline{H}_2$), 4.34–4.30 (m, 4H, C$\underline{H}_2$O-(C=O)), 3.76–3.73 (m, 4H, C$\underline{H}_2$CH$_2$O-(C=O)), 3.65 (s, 103H, C$\underline{H}_2$C$\underline{H}_2$O).
^{13}C-NMR (100 MHz, $CDCl_3$) δ 63.70 (C$\underline{H}_2$O-(C=O)), 69.12 (C$\underline{H}_2$CH$_2$O-(C=O)), 70.56 (C$\underline{H}_2$C$\underline{H}_2$O), 128.28 (C$\underline{H}$),, 131.04 (=C$\underline{H}_2$), 166.17 (C$\underline{=}$O).

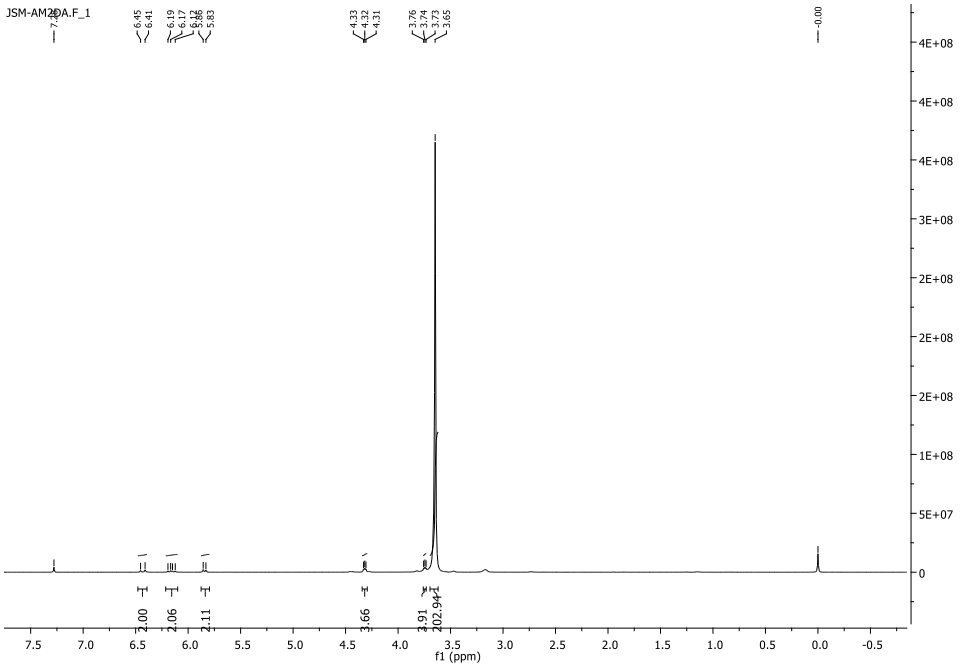

Figure 14. ^{1}H-NMR spectrum of PEG2000DA.

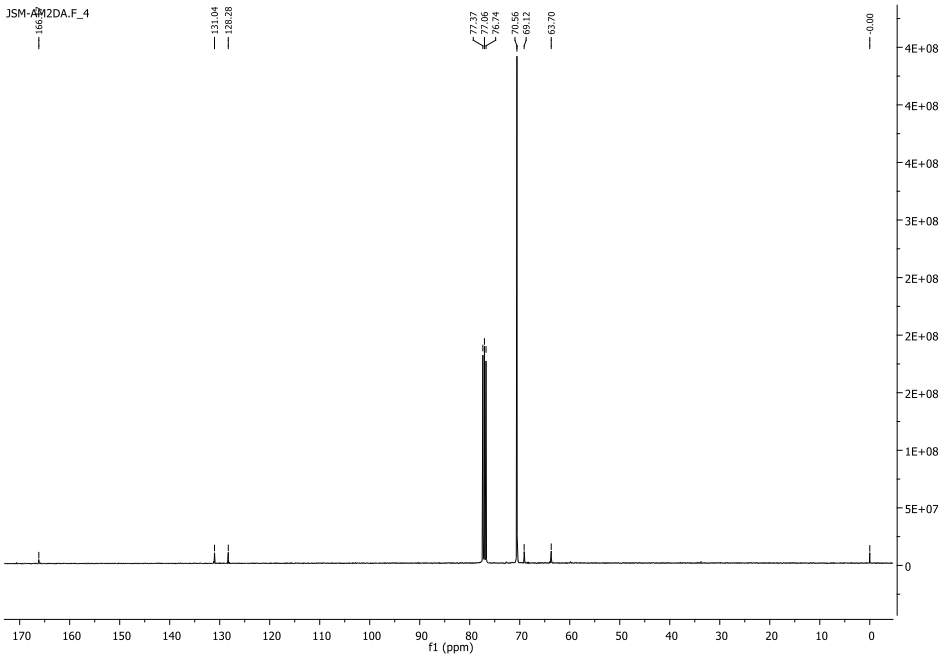

Figure 15. ^{13}C-NMR spectrum of PEG2000DA.

3.1.5. Poly(ethylene glycol) Diacrylate, PEG4000DA and PEG6000DA

Poly(ethylene glycol) (Mw = 4000 g mol^{-1}) (2 g, 0.5 mmol, 1 eq) was dissolved in CH_2Cl_2 (15 mL) and then triethylamine (0.20 g, 2 mmol, 4 eq) and acryloyl chloride (0.18 g,

2.0 mmol, 4 eq) were added. The reaction produced PEG4000DA (1.78 g, 0.43 mmol, 86 % yield) as a white waxy solid that foamed under vacuum.

The NMR assignments and structure determination were conducted using ^{1}H-NMR (Figure 16) and ^{13}C-NMR (Figure 17).

^{1}H-NMR (400 MHz, $CDCl_3$) δ 6.43 (d, *J* = 17.3 Hz,2H, =C$\underline{H}_2$), 6.16 (dd, *J* = 17.3, 10.4 Hz, 2H, =C$\underline{H}$), 5.84 (d, *J* = 10.4 Hz, 2H, =C$\underline{H}_2$), 4.33–4.29 (m, 4H, C$\underline{H}_2$O-(C=O)), 3.65 (s, 462H, C$\underline{H}_2$C$\underline{H}_2$O).
^{13}C-NMR (100 MHz, $CDCl_3$) δ 63.69 (C$\underline{H}_2$O-(C=O)), 69.11 (C$\underline{H}_2$CH$_2$O-(C=O)), 70.57 (C$\underline{H}_2$C$\underline{H}_2$O), 128.29 (C$\underline{H}$),131.00 (=C$\underline{H}_2$),166.14 (C$\underline{=}$O).

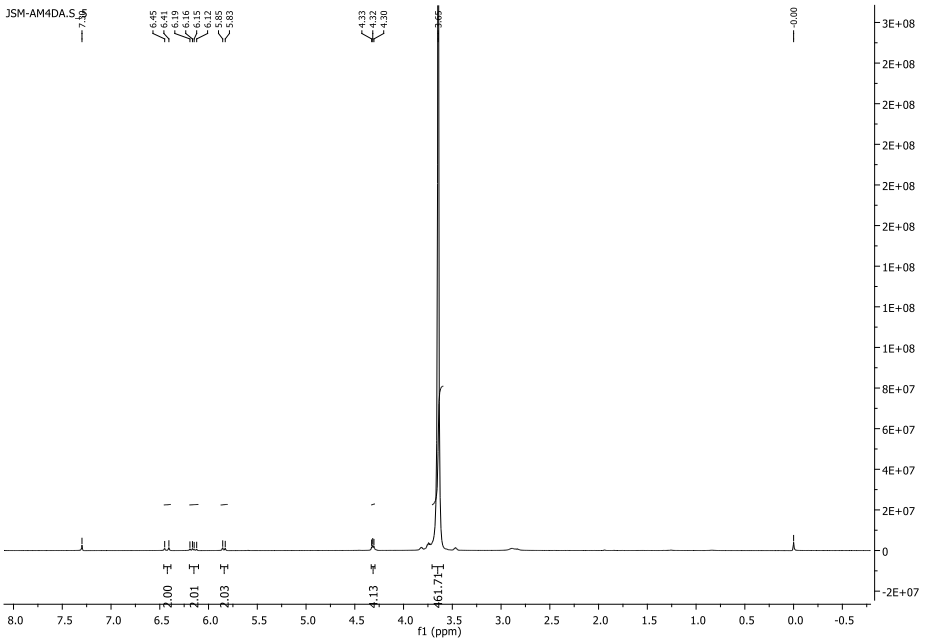

Figure 16. ^{1}H-NMR spectrum of PEG4000DA.

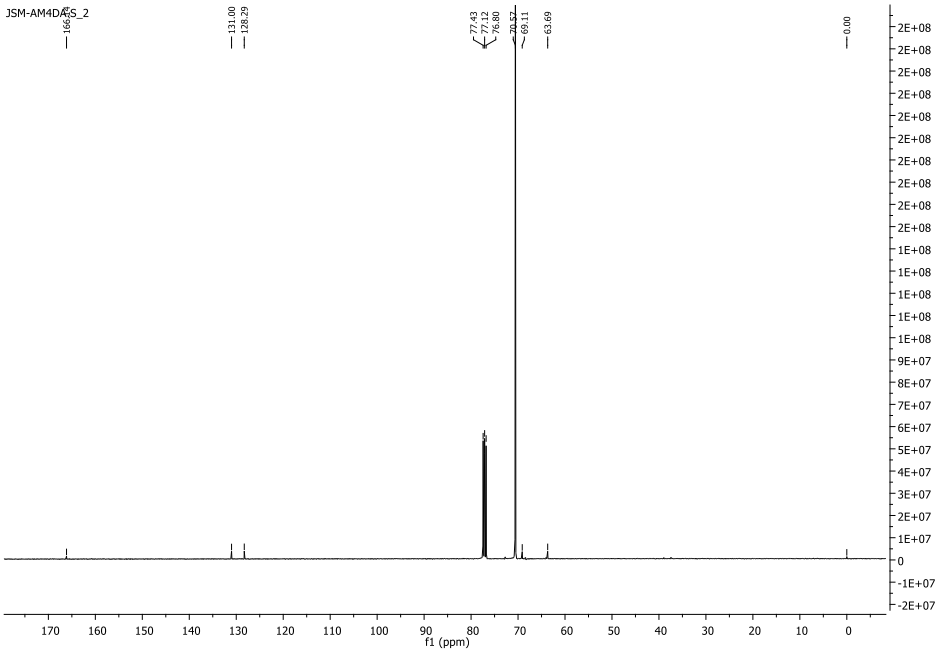

Figure 17. ^{13}C-NMR spectrum of PEG4000DA.

Poly(ethylene glycol) (Mw = 6000 g mol^{-1}) (2 g, 0.33 mmol, 1 eq) was dissolved in CH_2Cl_2 (15 mL) and then triethylamine (0.14 g, 1.33 mmol, 4 eq) and acryloyl chloride (0.12 g, 1.33 mmol, 4 eq) were added. The reaction produced PEG6000DA (1.48 g, 0.24 mmol, 73% yield) as a white waxy solid that foamed under vacuum.

The NMR assignments and structure determination were conducted using ^{1}H-NMR (Figure 18) and ^{13}C-NMR (Figure 19).

^{1}H-NMR (400 MHz, $CDCl_3$) δ 6.43 (d, *J* = 17.3 Hz, 2H, =C$\underline{H}_2$), 6.20–6.11 (m, 2H, =C$\underline{H}$), 5.84 (d, *J* = 10.4 Hz, 2H, =C$\underline{H}_2$), 4.33–4.30 (m, 4H, C$\underline{H}_2$O-(C=O)), 3.65 (s, 615H, C$\underline{H}_2$C$\underline{H}_2$O).
^{13}C-NMR (100 MHz, $CDCl_3$) ($CDCl_3$) δ 63.70 (C$\underline{H}_2$O-(C=O)), 69.11 (C$\underline{H}_2$C$\underline{H}_2$O-(C=O)), 70.55 (C$\underline{H}_2$C$\underline{H}_2$O), 128.28 (C$\underline{H}$),130.06 (=C$\underline{H}_2$),166.18 (C=O).

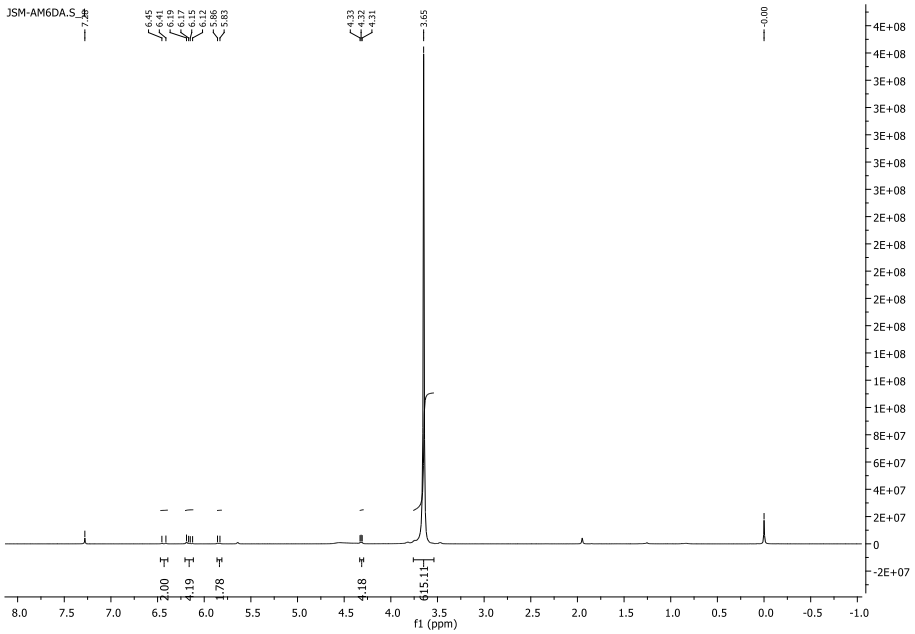

Figure 18. ^{1}H-NMR spectrum of PEG6000DA.

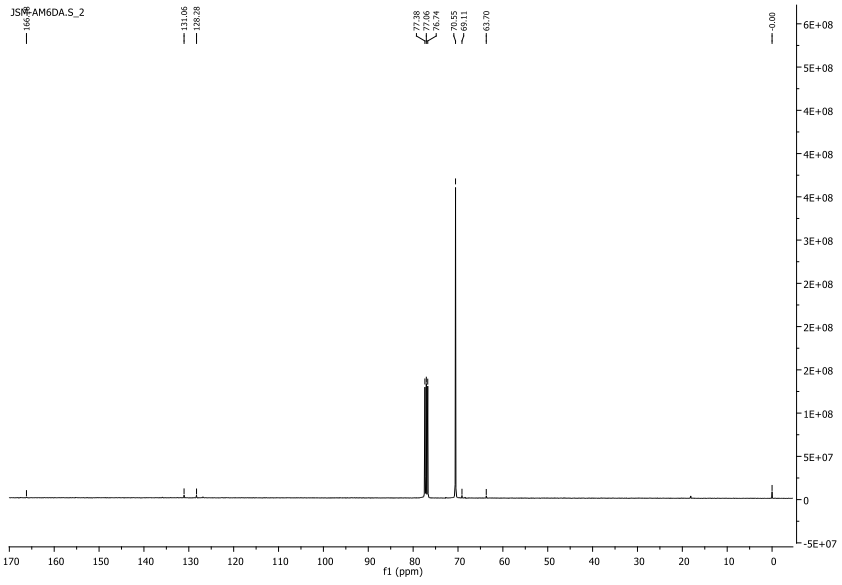

Figure 19. ^{13}C-NMR spectrum of PEG6000DA.

3.1.6. Poly(ethylene glycol) Diacrylate, PEG1000DA

The synthesis of PEG1000DA followed a similar procedure as described above for PEG1000DM, with the resulting crude product subsequently purified by column chromatography using EtOAC-hexane (5:1) followed by $CHCl_3$:MeOH (9:1). Compounds were visualized using phosphomolybdic acid by TLC analysis ($CHCl_3$-MeOH 9:1).

Poly(ethylene glycol) (Mw = 1000 g mol^{-1}) (2 g, 2 mmol, 1 eq) was dissolved in CH_2Cl_2 (15 mL), and then triethylamine (0.81 g, 8 mmol, 4 eq) and acryloyl chloride (0.73 g, 8 mmol, 4 eq) were added. The reaction produced PEG1000DA (2.02 g, 1.82 mmol, 91% yield) as a yellow waxy solid that foamed under vacuum.

The NMR assignments and structure determination were conducted using ^{1}H-NMR (Figure 20), ^{13}C-NMR (Figure 21), Dept (Figure 22), and using two-dimensional NMR (COSY (Figure 23) and HSQC (Figure 24)).

^{1}H-NMR (400 MHz, $CDCl_3$) δ 6.43 (d, *J* = 17.3 Hz, 2H, =C$\underline{H}_2$), 6.16 (dd, *J* = 17.4, 10.4 Hz, 2H, =C$\underline{H}$), 5.84 (d, *J* = 10.4 Hz, 2H, =C$\underline{H}_2$), 4.34–4.29 (m, 4H, C$\underline{H}_2$O-(C=O)), 3.77–3.72 (m, 4H, C$\underline{H}_2$C$\underline{H}_2$O-(C=O)), 3.64 (s, 86H, C$\underline{H}_2$C$\underline{H}_2$O).
^{13}C-NMR (100 MHz, $CDCl_3$) δ 63.68 (C$\underline{H}_2$O-(C=O)), 69.10 (C$\underline{H}_2$CH$_2$O-(C=O)), 70.55 (C$\underline{H}_2$C$\underline{H}_2$O), 128.28 (C$\underline{H}$) 130.98 (=C$\underline{H}_2$), 166.12 (C$\underline{=}$O).

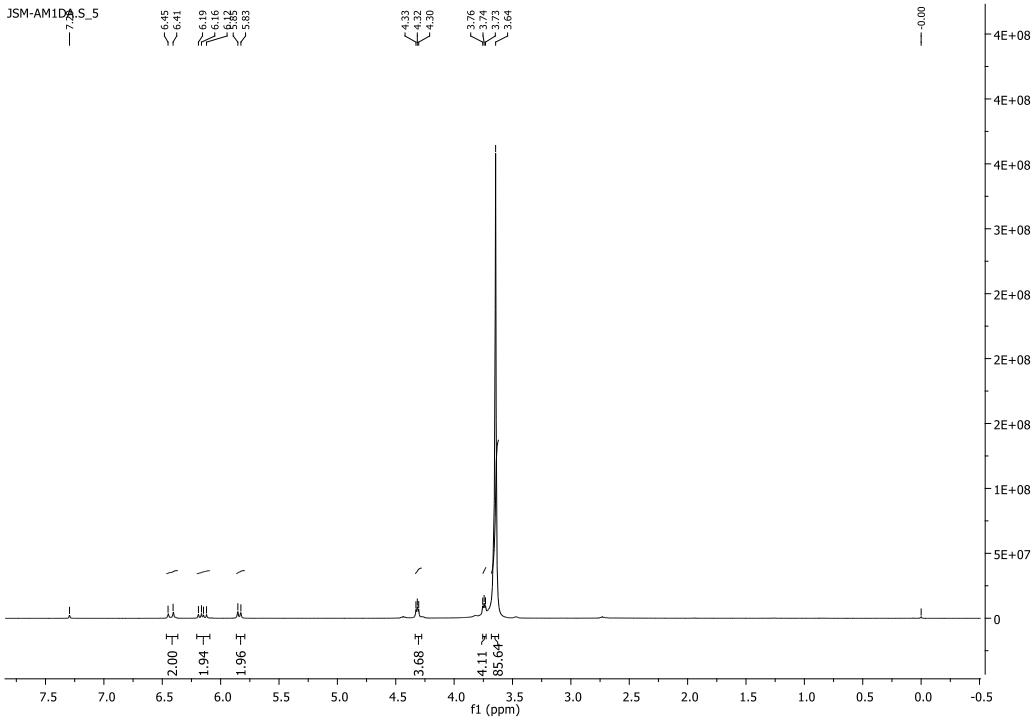

Figure 20. ^{1}H-NMR spectrum of PEG1000DA.

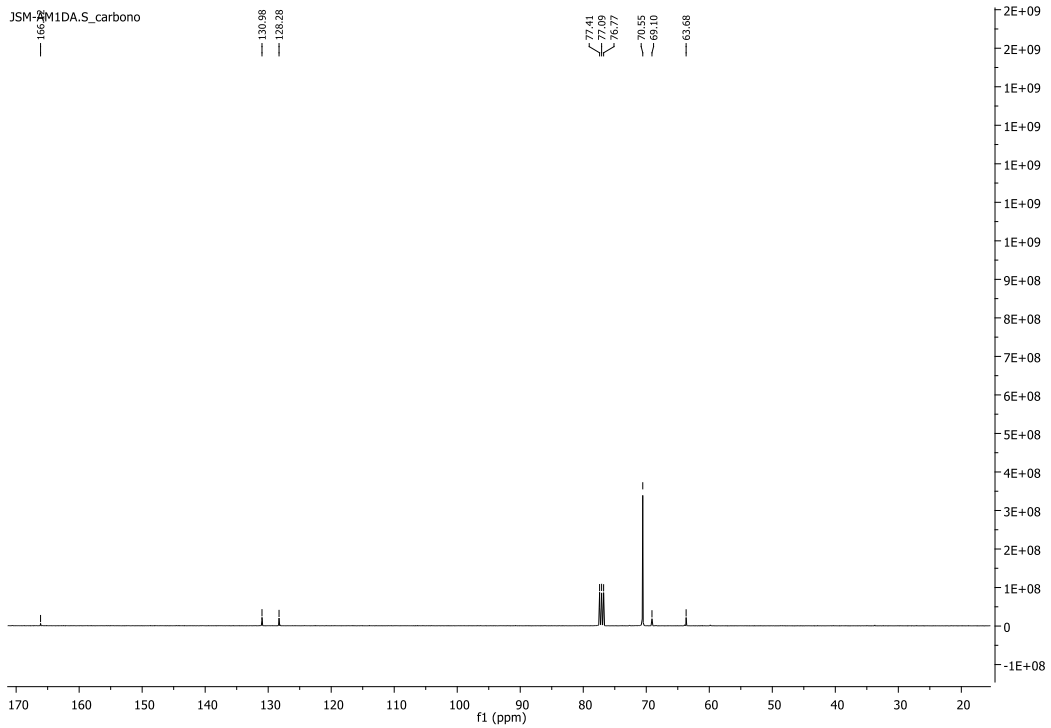

Figure 21. ^{13}C-NMR spectrum of PEG1000DA.

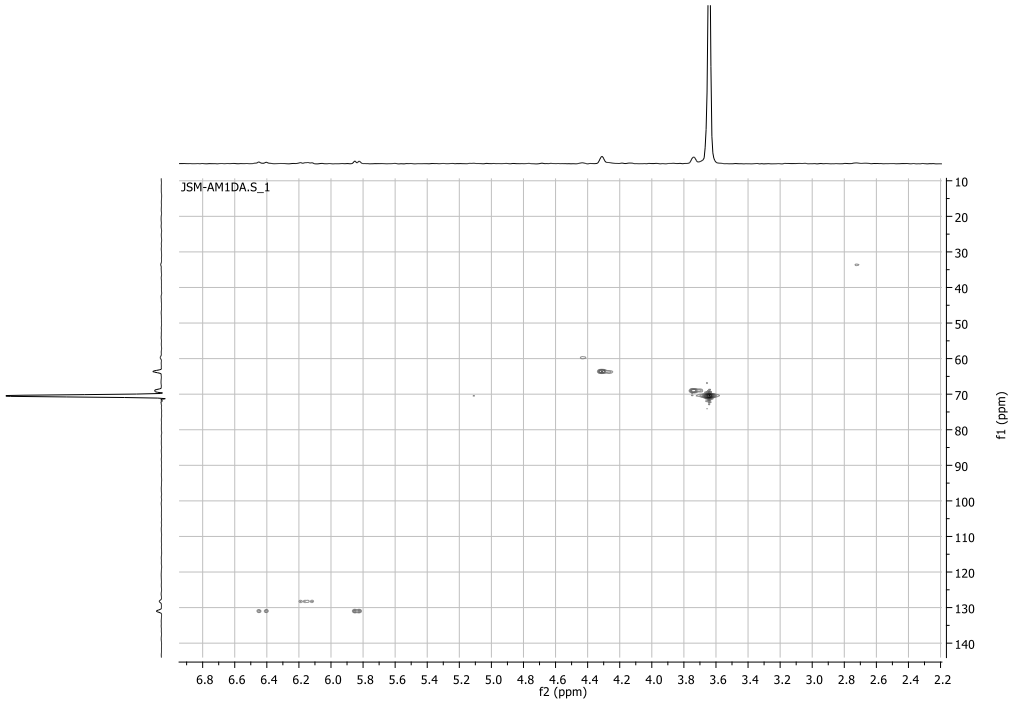

Figure 22. HSQC spectrum of PEG1000DA.

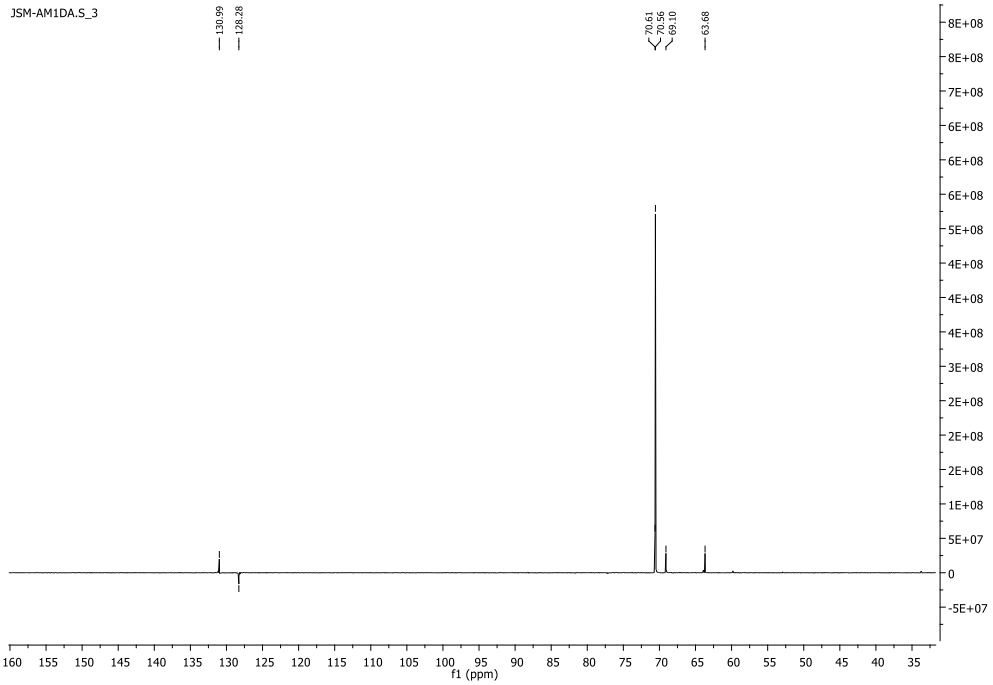

Figure 23. ^{13}C DEPT NMR spectrum of PEG1000DA.

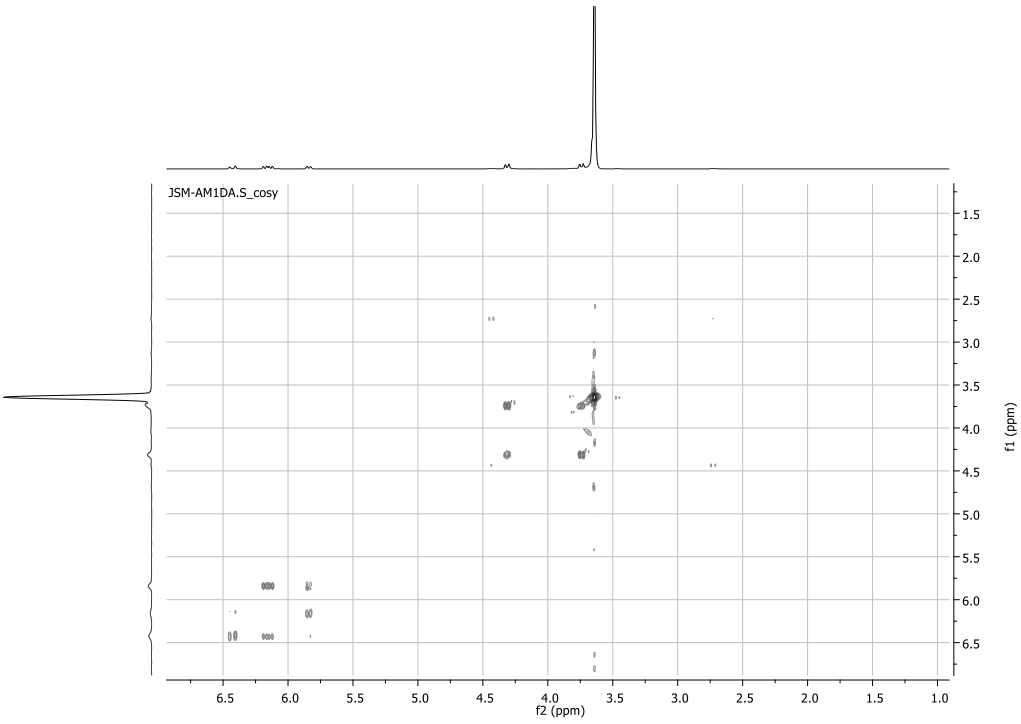

Figure 24. COSY spectrum of PEG1000DA.

3.1.7. MALDI-TOF MS

Quantitative functional group transformations are crucial in PEG end group modifications due to the challenges associated with isolating products from PEGs (starting materials). However, conventional characterization techniques like NMR spectroscopy face limitations in assessing the efficiency of end group transformations. This limitation arises from the overwhelming signal of the PEG backbone protons, which tends to overshadow the signals originating from the end groups [17,18]. While NMR spectroscopy

can confirm the addition of end groups, the low proportion of these signals relative to the PEG backbone complicates determining the completion of the reaction solely through 1H-NMR integration.

Although the NMR spectra of products may display expected peaks and the absence of additional peaks, indicating the quantitative removal of unreacted (meth)acryloyl chloride and trimethylamine, the distinction between unreacted PEG and partially reacted species remains challenging due to the overlapping signals of PEG protons [19]. While MALDI-TOF MS may not reveal low-molecular-weight impurities, it proves invaluable in providing data for end group analysis [20].

MALDI-TOF MS proves invaluable in discerning macromolecules with identical repeating unit structures but differing end groups, thereby confirming high-end group purity [17,18]. Upon ionization, MALDI-TOF detects singly charged, structurally intact macromolecules, often presenting a Gaussian distribution. Consequently, the mass, average molecular weights (Mn and Mw), and polydispersity (PDI) of macromolecules can be accurately determined. The arrangement of macromolecules in the spectra typically reflects the mass of the repeat unit, with each observed signal containing end group information.

In cases where two macromolecules differ solely in the type and mass of their end groups, their MALDI-TOF mass spectra exhibit distinct series of m/z peaks, referred to as the main and minor series of peaks, with each set separated by the mass of the repeat unit [17,18]. The increase in mass observed in individual peaks of product materials compared to starting materials corresponds to the addition of the masses of the end groups.

The MALDI-TOF mass spectra of both the starting materials and resulting products are depicted in Figures 25 and 26, respectively. Typically, end-group analysis utilizing MALDI-TOF mass spectrometry yields two sets of peaks post-esterification: a predominant main series of peaks and a minor series. The presence of this minor series may indicate the presence of unreacted PEG post-reaction, or it could suggest that some molecules within the distribution have been functionalized by a single end group rather than two. On average, adjacent peaks within the same series exhibit a mass difference of 44 Da (Dalton), corresponding to the molecular mass of the oxyethylene repeat unit.

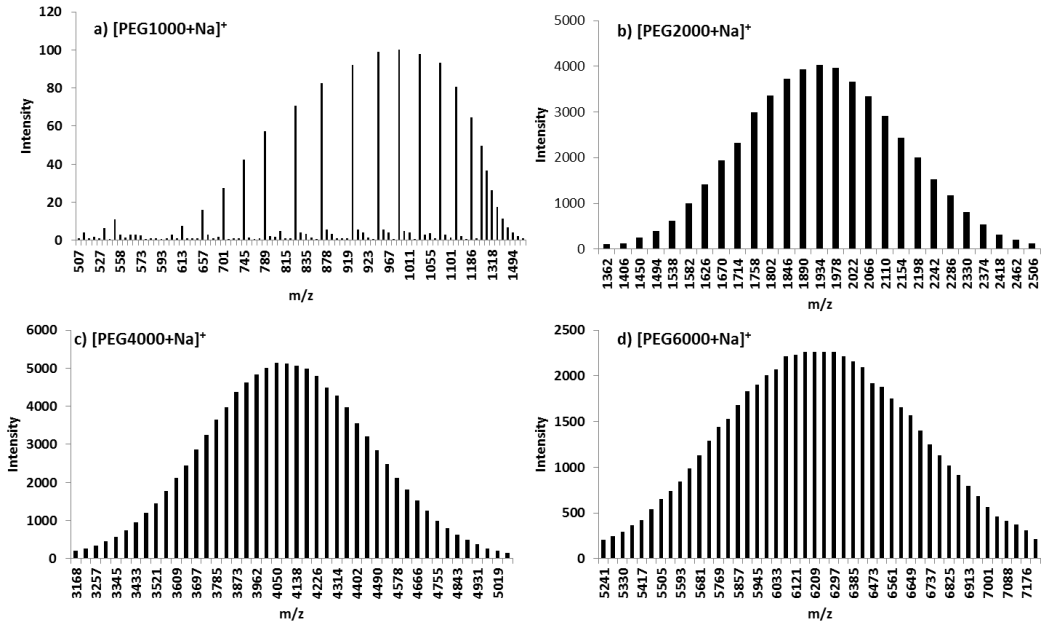

Figure 25. MALDI-TOF mass spectra of $[PEG+Na]^+$: (**a**) $[PEG1000+Na]^+$, (**b**) $[PEG2000+Na]^+$, (**c**) $[PEG4000+Na]^+$, (**d**) $[PEG6000+Na]^+$.

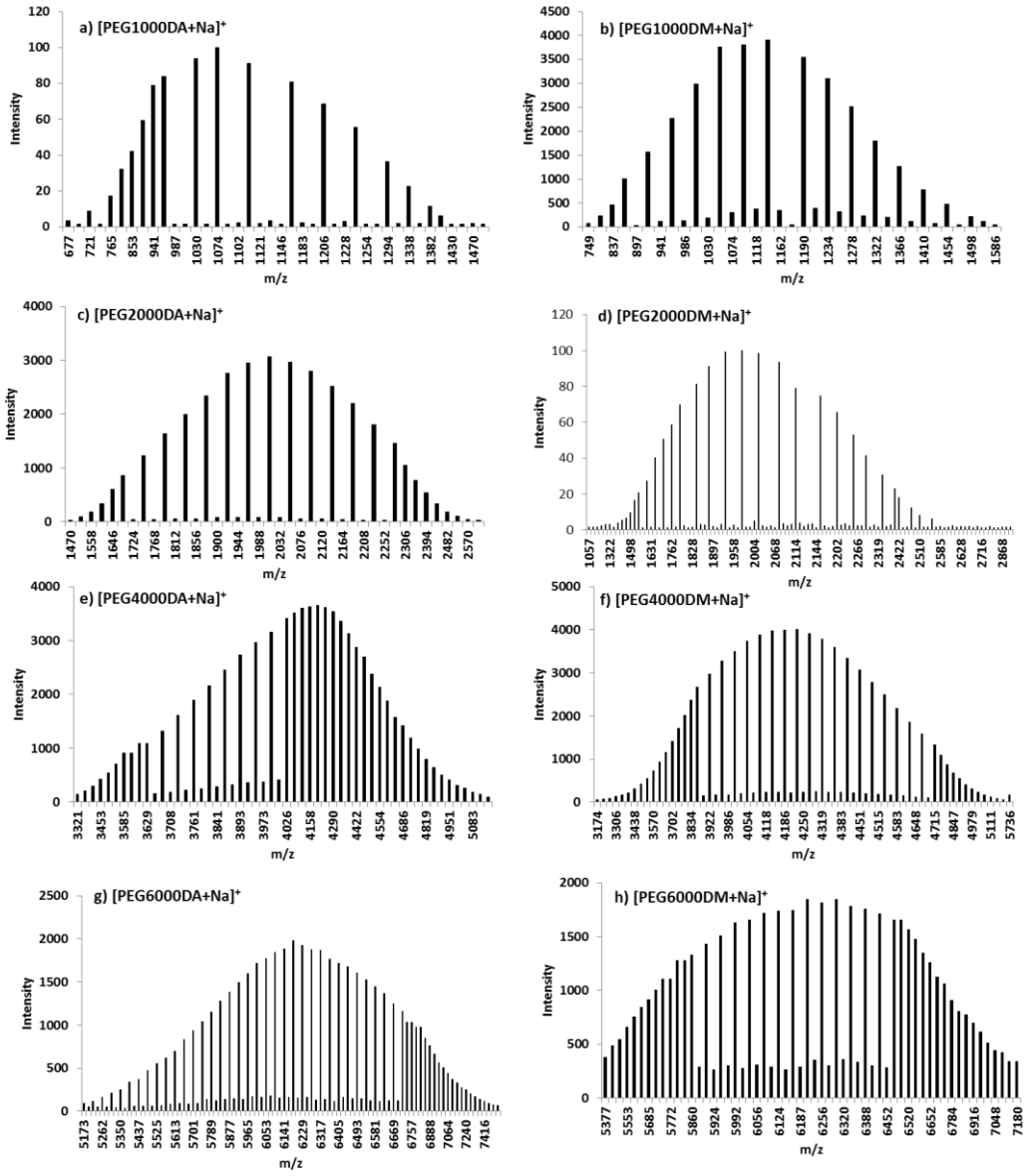

Figure 26. MALDI-TOF mass spectra of [PEG di(meth)acrylate+Na]$^+$: (**a**) [PEG1000DA+Na]$^+$, (**b**) [PEG1000DM+Na]$^+$, (**c**) [PEG2000DA+Na]$^+$, (**d**) [PEG2000DM+Na]$^+$, (**e**) [PEG4000DA+Na]$^+$, (**f**) [PEG4000DM+Na]$^+$, (**g**) [PEG6000DA+Na]$^+$, (**h**) [PEG6000DM+Na]$^+$.

The main series data, including average molecular weights (Mn and Mw), polydispersity (PDI), and the number of ethylene oxide units (n), are presented in Table 1. Calculated molecular weights were derived from the molecular weights of the corresponding starting PEG materials. Post-esterification, it was anticipated that each peak in the product would exhibit a mass shift corresponding to the end groups, as observed in the MALDI-TOF mass spectrum compared to individual peaks of the starting material.

Table 1. The theoretical and observed molecular weights of starting material $[PEG+Na]^+$ and resulting products obtained from MALDI-TOF measurements for the main series of peaks.

[Macromolecule+Na]$^+$	M_n		M_w		PDI	
	Observed	Theoretical	Observed	Theoretical	Observed	Theoretical
$[PEG1000+Na]^+$	1011.34	-	1044.01	-	1.03	-
$[PEG1000DA+Na]^+$	1062.75	1062.68	1084.73	1084.67	1.02	1.02
$[PEG1000DM+Na]^+$	1137.92	1137.74	1156.87	1156.69	1.02	1.02
$[PEG2000+Na]^+$	1940.94	-	1963.25	-	1.01	-
$[PEG2000DA+Na]^+$	2013.90	2013.89	2033.02	2033.02	1.01	1.01
$[PEG2000DM+Na]^+$	1998.66	1998.81	2021.92	2022.01	1.01	1.01
$[PEG4000+Na]^+$	4097.09	-	4127.30	-	1.01	-
$[PEG4000DA+Na]^+$	4192.30	4192.13	4221.02	4220.87	1.01	1.01
$[PEG4000DM+Na]^+$	4202.99	4201.59	4231.52	4228.36	1.01	1.01
$[PEG6000+Na]^+$	6235.73	-	6264.05	-	1.01	-
$[PEG6000DA+Na]^+$	6276.09	6277.45	6308.06	6305.82	1.01	1.01
$[PEG6000DM+Na]^+$	6254.18	6255.21	6278.75	6279.79	1.00	1.00

A strong correlation was noted between the average difference observed in individual peak values for PEGDMs and PEGDAs and their respective theoretical values. The main series corresponds to di-functionalized Na+ cationized PEG.

The calculated mass m(n) of the most intense peak follows a linear function of a number of the polymer repeat unit (n):

$$m(n) = n\, m_{monomer} + m_{end\ groups} + m_{cation}$$

Here, n represents the number of ethylene oxide repeat units, $m_{monomer}$ stands for the mass of the repeat unit, m_{end} groups denotes the residue mass of both end groups, and m_{cation} represents the mass of the sodium cation. The major peaks and their corresponding masses are utilized to calculate the number of repeat units (as shown in Table 1).

For the starting material PEG ($HO\text{-}(CH_2CH_2O)_n\text{-}H$), the theoretical peak mass can be expressed as $m(n) = n \times 44.053 + 17.007 + 1.008 + 22.990$ (where n (the molecular weight of ethylene oxide) + (the molecular weight of the hydroxyl terminal group) + (the molecular weight of the hydrogen terminal group) + (the molecular weight of the sodium cation)).

Similarly, for the dimethacrylate PEG ($((CH_3CH_2C)OCO\text{-}(CH_2CH_2O)_n\text{-}COC(CH_2CH_3))$, the theoretical expression is $m(n) = n \times 44.053 + 85.082 + 69.083 + 22.990$, and for the di-acrylate PEG ($((HCH_2C)OCO\text{-}(CH_2CH_2O)_n\text{-}COC(CH_2H))$, it is $m(n) = n \times 44.026 + 71.055 + 55.066 + 22.990$.

For example, considering the theoretical mass value of 22 repeat units in $[PEG1000+Na]^+$, it corresponds to $22 \times 44.053 + 18.015 + 22.990 = 1010.17$ Da, which closely aligns with the observed mass for $n = 22$ of 1009.49 Da. Similarly, for PEG1000DA, the difference between the theoretical (1118.27 Da) and observed (1117.56 Da) mass is just 0.71 Da. Theoretical calculations and observed distributions are detailed in Table 2. The proximity of expected masses to observed masses indicates minimal contamination.

Table 2. Calculated and experimental mass m(n) of the most intense peak in each [macromolecule+Na]$^+$ spectrum.

[Macromolecule+Na]$^+$	n	Calculated m(n)	Experimental m(n)
[PEG1000+Na]$^+$	22	1010.17	1009.49
[PEG1000DA+Na]$^+$	22	1118.27	1117.56
[PEG1000DM+Na]$^+$	21	1102.27	1101.65
[PEG2000+Na]$^+$	43	1935.28	1934.13
[PEG2000DA+Na]$^+$	41	1955.27	1954.09
[PEG2000DM+Na]$^+$	42	2027.38	2025.97
[PEG4000+Na]$^+$	91	4049.83	4049.67
[PEG4000DA+Na]$^+$	92	4201.98	4201.87
[PEG4000DM+Na]$^+$	92	4230.03	4230.51
[PEG6000+Na]$^+$	142	6296.53	6297.09
[PEG6000DA+Na]$^+$	137	6184.36	6184.65
[PEG6000DM+Na]$^+$	138	6256.47	6256.15

From a minor set of peaks with much lower intensity, specifically observed in Figure 26c) (approximately 1700–2250 m/z), (e) (approximately 3600–4000 m/z), and (f) (approximately 3800–4700 m/z), a residual amount of mono-functionalized PEG species was identified (refer to Table 3). However, it can be inferred from the intensity of the peak series that high reaction conversions were attained.

Table 3. The theoretical and observed molecular weights of [PEG2000A+Na]$^+$, [PEG4000A+Na]$^+$, and [PEG4000M+Na]$^+$ obtained from MALDI-TOF measurements for minor series of peaks (if only one end of PEG was functionalized).

[Macromolecule+Na]$^+$	Mn		Mw		PDI	
	Observed	Theoretical	Observed	Theoretical	Observed	Theoretical
[PEG2000A+Na]$^+$	1975.06	1975.07	1985.35	1985.34	1.01	1.01
[PEG4000A+Na]$^+$	3873.62	3872.15	3876.69	3876.69	1.01	1.00
[PEG4000M+Na]$^+$	4276.44	4275.73	4287.69	4286.97	1.00	1.00

4. Discussion

4.1. Differential Scan Calorimetry Results

The thermal behavior of the synthesized PEG-di-functionalized compounds was examined over a temperature range spanning from −80 °C to 130 °C, with heating and cooling rates of 5 and 20 °C min^{-1}, respectively. Details regarding temperatures and enthalpies are provided in Table 4. Thermal analysis of the corresponding polymers was initiated within the DSC furnace.

In the case of PEG1000, the macromolecular chains are sufficiently long and mobile to facilitate the formation of ordered arrangements, leading to crystallization characterized by a distinct exothermic peak followed by a broad endothermic peak corresponding to the melting of the previously formed crystalline fraction (refer to Figure 27a). Subsequent heating and cooling cycles revealed recurring crystallization and melting events, indicative of a crystalline macromolecule.

Table 4. Thermal properties of PEG macromolecules obtained by DSC during two cooling/heating cycles. Tg-glass transition temperature; Tm—melting temperature; Tc-crystallization temperature; ΔHm and ΔHc-melting and crystallization enthalpies, respectively.

Sample		Cooling Scan			Heating Scan		
		Glass Transition	Melt-Crystallization		Glass Transition	Melting	
	scan	Tg/°C	Tc/°C	ΔHcr/J g-1	Tg/°C	Tm/°C	ΔHm/J g^{-1}
PEG1000	I	-	28.61	152.8		37.37	153.8
	II	-	27.73	154.6		31.59/38.55	160.5
	III					38.50	161.3
PEG1000DA oligomer	I	-	-	-		36.66	127.1
PEG1000DA polymer	I	−50.68	-	-	−48.41	-	-
	II	−51.56	-	-	−48.50	-	-
PEG1000DM oligomer	I	-	-	-	-	23.52	101.8
PEG1000DM polymer	I	−51.00	-	-	−45.71	-	-
	II	−51.09	-	-	−44.89	-	-
PEG2000	I	-	32.79	163.5	-	53.96	174.8
	II	-	35.52	163.8	-	53.67	166.6
	III	-	-	-	-	53.65	166.6
PEG2000DA oligomer	I	-	-	-	-	52.25	141.8
PEG2000DA polymer	I	-	24.65	70.24	-	41.64	69.28
	II		24.88	75.05	-	42.25	70.52
PEG2000DM oligomer	I	-	-	-	-	55.38	140.9
PEG2000DM polymer	I	-	24.65	70.24		41.64	69.28
	II	-	24.88	75.05		42.25	70.52
PEG4000	I	-	41.58	180.8		62.27	199.4
	II	-	41.95	181.5		61.36	186.0
	III	-	-	-		61.36	186.7
PEG4000DA oligomer	I	-	-	-	-	57.91	176.2
PEG4000DA polymer	I	-	24.92	72.32	-	41.43	72.05
	II	-	25.24	73.21	-	41.59	73.69
PEG4000DM oligomer	I	-	-	-	-	50.36	134.8
PEG4000DM polymer	I	-	16.78	55.61	-	35.42	52.93
	II	-	18.56	58.85	-	35.42	52.93
PEG6000	I	-	38.90	164.4	-	62.91	171.5
	II	-	38.46	163.2	-	62.80	168.85
	III	-	-	-	-	62.87	167.9
PEG6000DA oligomer	I	-	-	-	-	59.01	76.31
PEG6000DA polymer	I	-	31.06	74.87	-	42.63	76.31
	II	-	31.53	76.67	-	42.97	77.14
PEG6000DM oligomer	I	-	-	-	-	54.88	149.5
PEG6000DM polymer	I	-	38.81	80.14	-	48.34	77.85
	II		34.83	86.52	-	49.14	77.79

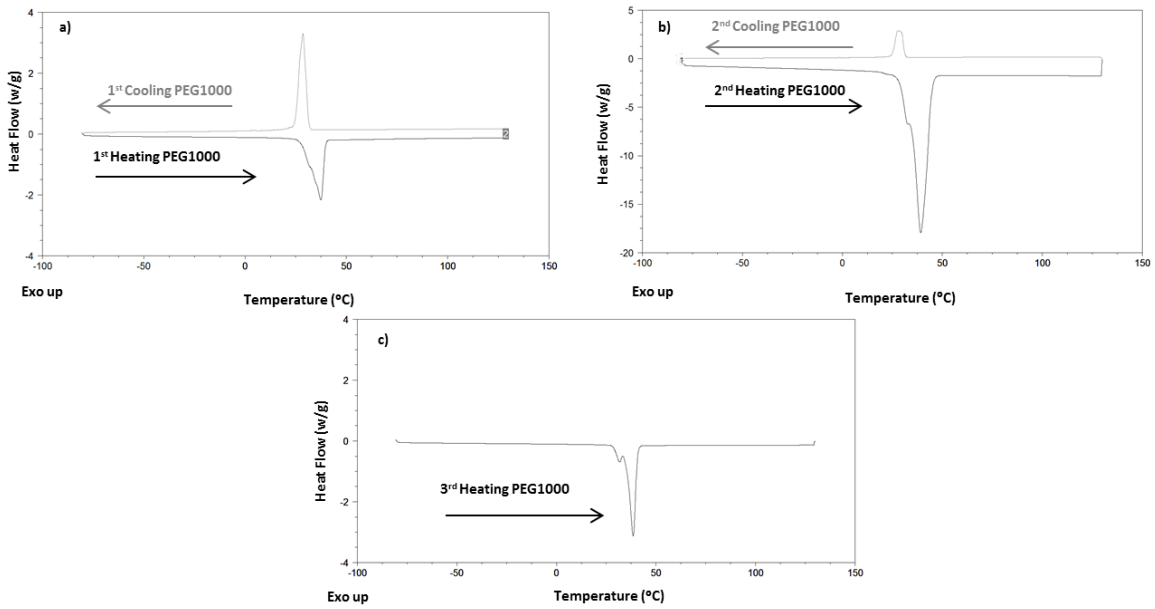

Figure 27. Thermograms (heat flow vs. temperature) of PEG1000 collected at three heating and two cooling cycles at 5 °C min^{-1}. (**a**) first heating and first cooling cycles; (**b**) second heating and second cooling cycles; (**c**) third heating cycle.

For the PEG1000DM polymer, following the melting of the oligomer (PEG1000DM) with 1 wt.% of AIBN, the temperature increases once more during heating until an exothermic effect attributed to polymerization occurs (refer to Figure 28a). Subsequent heating and cooling cycles reveal a polymer glass transition temperature at −45.3 °C, with no further thermal processes observed, indicating a fully amorphous polymer state (Figure 28b,c). Consequently, the presence of crosslinks in the polymer reduces its crystallinity compared to the starting PEG1000. The formation of crosslinks hinders polymer chain sliding diffusion and disentanglement, limiting the ability of chains to rearrange into an ordered morphology as observed in the macromolecule PEG1000. Similarly, the PEG1000DA polymer exhibits the same amorphous behavior as the PEG1000DM polymer (as outlined in Table 4).

This divergence in crystallization behavior between the polymer network and the corresponding macromolecules arises from the presence of crosslinks, which decrease the critical chain length required for crystallization. As a result, the molecular chains are no longer of sufficient length to undergo crystallization. Additionally, the presence of crosslinks restricts the freedom of the chains to rearrange into a crystalline conformation [10,13]. Consequently, the thermal behavior of the PEG1000 polymer differs from that of the corresponding PEG1000 oligomers.

The thermal analysis of the PEG2000DM polymer (Figure 29a–c) indicates that the sample exceeds the critical molecular chain length necessary for crystallization. As a result, crystal morphology is observed, indicating that the chain length is sufficient for folding and crystallization despite polymer cross-linking. Consequently, the PEG2000DM polymer exhibits a crystallization behavior similar to that of the starting material PEG2000 (Figure 30).

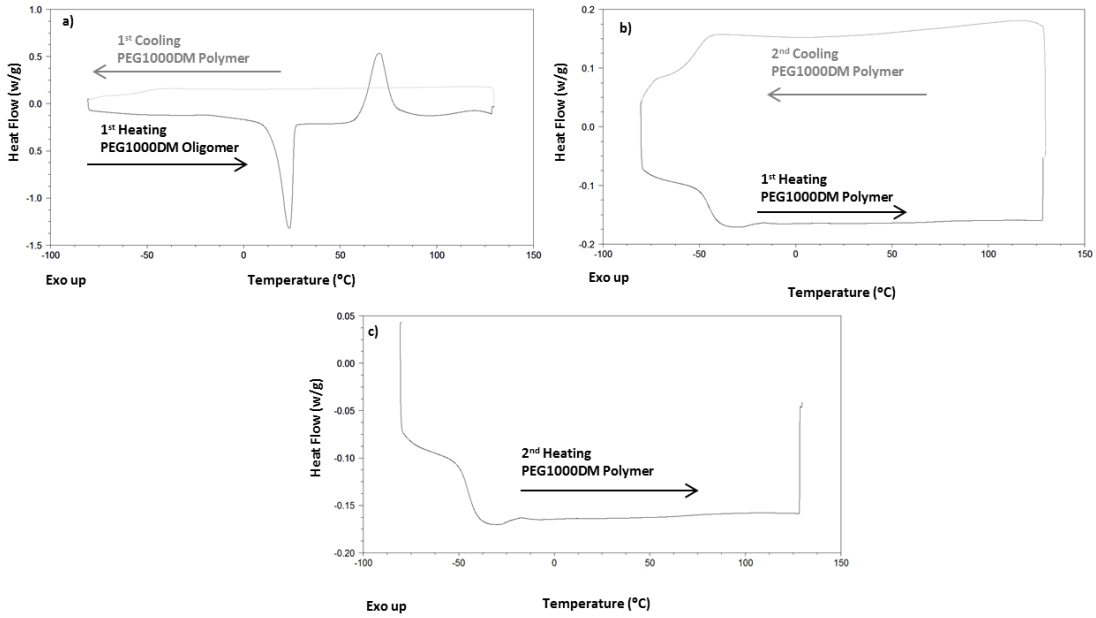

Figure 28. Thermograms (heat flow vs. temperature) obtained for a mixture of PEG1000DM oligomer with 1 wt.% of AIBN collected at the heating scan at 5 °C min^{-1} and PEG1000DM polymer collected at two heating and cooling cycles at 5 °C min^{-1}. (**a**) first heating cycle for the oligomer and first cooling cycle for the polymer; (**b**) first heating cycle and second cooling cycle for the polymer; (**c**) second heating cycle for the polymer.

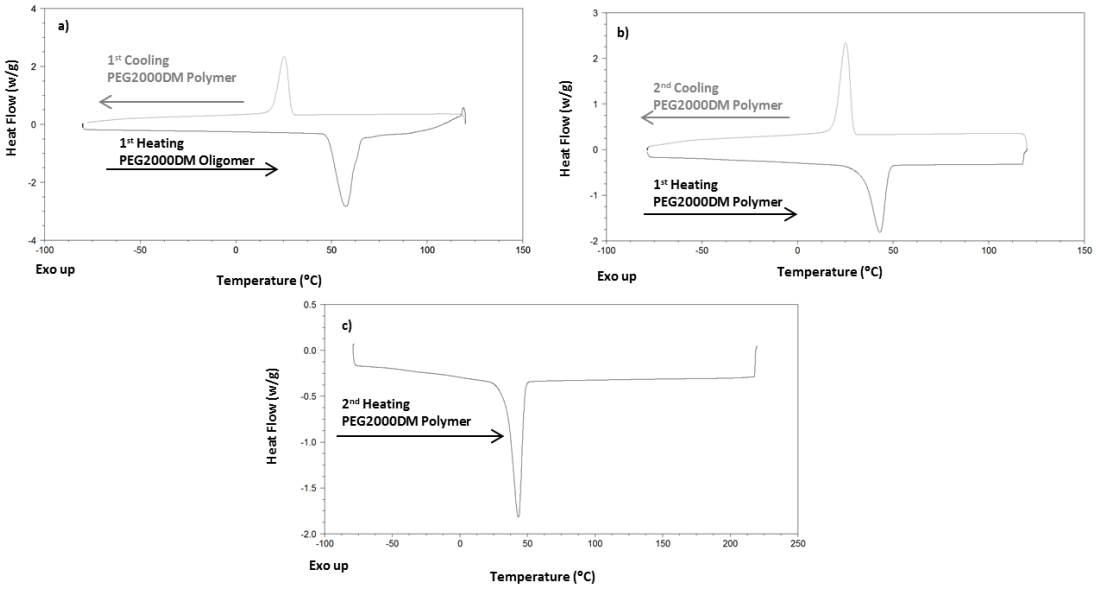

Figure 29. Thermograms (heat flow vs. temperature) obtained for a mixture of PEG2000DM oligomer with 1 wt.% of AIBN collected at the heating scan at 5 °C min^{-1} and PEG2000DM polymer collected at two heating and cooling cycles at 5 °C min^{-1}. (**a**) first heating cycle for the oligomer and first cooling cycle for the polymer; (**b**) first heating cycle and second cooling cycle for the polymer; (**c**) second heating cycle for the polymer.

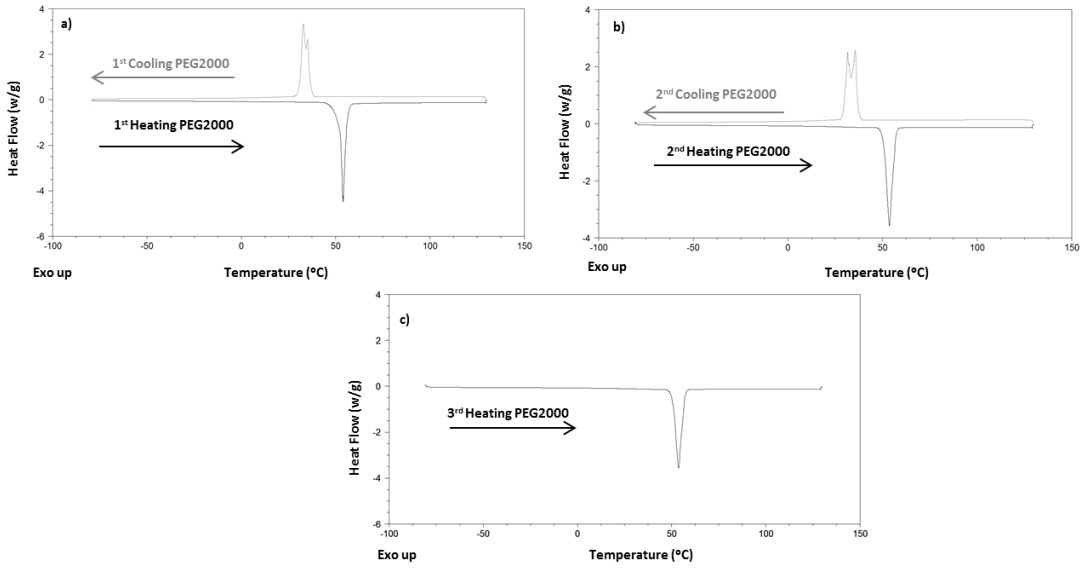

Figure 30. Thermograms (heat flow vs. temperature) of PEG2000 collected at three heating and two cooling cycles at 5 °C min^{-1}. (**a**) first heating and first cooling cycles; (**b**) second heating and second cooling cycles; (**c**) third heating cycle.

While the glass transition of the PEG2000 polymer is not detected (as observed in Figure 29), it is conceivable that the polymer exists in a semi-crystalline state with portions of chains residing in an amorphous region. The glass transition of highly crystalline macromolecules can be exceedingly subtle and challenging to discern due to the dominance of the crystalline phase [4]. The introduction of cross-links in the polymer matrix reduces crystal perfection and crystal size by constraining chain mobility [10,13], consequently resulting in a reduction in melting temperature from 54 °C in PEG2000 (as depicted in Figure 30) to 42 °C in the PEG2000DM polymer (as shown in Figure 29).

Moreover, an increase in chain length can hinder the crystallization process by augmenting chain friction, thereby impeding chain rearrangement into a regular crystalline morphology [11]. Consequently, it is expected that these samples crystallize with a larger proportion of chains in the amorphous phase [4]. While direct evidence of this behavior is not explicitly presented in the DSC thermograms collected for PEG4000 and PEG6000 and their corresponding polymers (as detailed in Table 4), they exhibit a similar behavior to PEG2000 and its respective polymers.

It is important to note that macromolecules with varying chain lengths may crystallize in different crystal forms with varying degrees of crystal arrangements, resulting in species melting at different temperatures [4,21,22]. This phenomenon is confirmed by the observation of double endothermic peaks at 31.59 °C and 38.55 °C during the second and third heating scans in the DSC curves of the PEG1000 sample. Imperfect crystals may melt at 37.37 °C in a broad peak during the first heating scan (as illustrated in Figure 27a), transitioning into different size distributions of crystals through melt-crystallization, subsequently melting later in two double peaks (as depicted in Figure 27c). Similarly, in the DSC curves of the PEG2000 sample (as shown in Figure 30a,b), a double-crystallization peak is observed at 32.74 °C and 35.22 °C, confirming the presence of different crystal sizes. However, in the DSC curves of the corresponding polymers, the double peaks transition into a single peak due to modifications in the polymer crystal structure induced by cross-linking. These cross-links promote the formation of more imperfect crystals with greater dimensions, which are reflected in the appearance of a single peak.

4.2. Electro-Optical Results

The electric-field-transmittance curves, representing the variation in transmittance as a function of PEG polymer chain length, are depicted in Figure 31, with corresponding electro-optical parameters summarized in Table 5. The thermal PDLCs were prepared through thermal polymerization at 70 °C, conducted overnight.

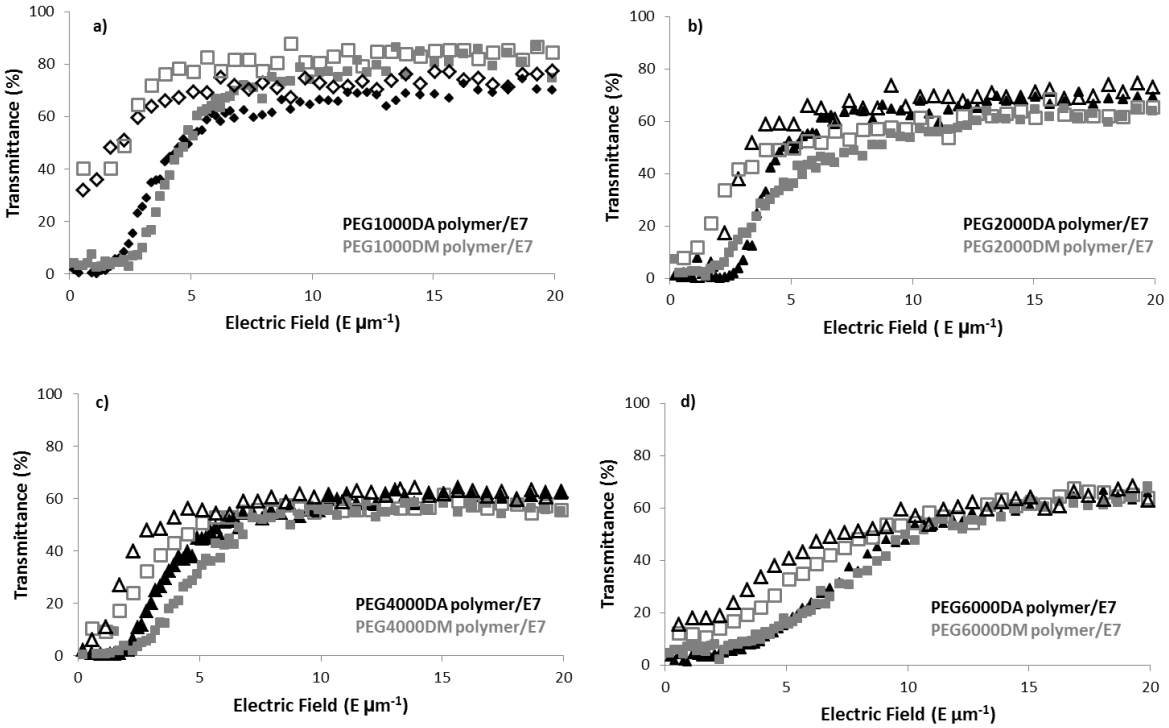

Figure 31. The electro-optical response of PDLC films prepared with 30 wt.% of (**a**) PEG1000DA, PEG1000DM, (**b**) PEG2000DA, PEG2000DM, (**c**) PEG4000DA, PEG4000DM, (**d**) PEG6000DA and PEG6000DM, with 1 wt.% of AIBN and 70 wt.% of E7, polymerized at 70 °C overnight. The transmittance was measured by applying the electrical field (filled symbols) and after removing the electric field (open symbols).

Table 5. Electro-optical properties of the PDLCs films prepared from 30 wt.% of PEG pre-polymer with 1 wt.% of AIBN and 70 wt.% of E7.

PDLC Polymer	T_0 (%)	T_{OFF} (%)	T_{max} (%)	PME (%)	MSC (%)	E_{90} (V µm^{-1})
PEG1000DA	1.6	32	73	43	31	8.63
PEG1000DM	5.3	30	84	31	24	11.78
PEG2000DA	0.9	1.5	67	0.9	0.6	6.15
PEG2000DM	7.3	8.7	65	2.5	1.4	10.53
PEG4000DA	2.7	6	56	5.5	3.3	5.5
PEG4000DM	0.3	10	57	17	9.7	7.02
PEG6000DA	1.8	15.6	64	22	14	13.76
PEG6000DM	4.7	12.3	63	13	7.6	13.45

These results are closely linked to the thermal characteristics of the polymer matrix. It is evident that for PDLCs incorporating amorphous, flexible PEG1000 polymer chains (as illustrated in Figure 31a), with average glass transition temperatures (Tg) of −48.46 °C (for PEG1000DA polymer) and −45.30 °C (for PEG1000DM polymer), the transmittance in the OFF state after the scan-down cycle does not revert to its original scattering state, but instead retains a transmittance state, averaging around 30%.

In contrast, PDLCs prepared with longer polymer chains tend to adopt crystalline structures, resulting in increased rigidity that inhibits the permanent memory effect (PME), as illustrated in Figure 1. Consequently, the transmittance reverts to a scattering state upon removal of the applied electric field.

The percentage of permanent memory effect (PME) can be calculated by the equation:

$$\%(\text{PME}) = \frac{T_{OFF} - T_0}{T_{MAX} - T_0} \times 100$$

where T_0 is the transmittance for the initial opaque state (zero electric field), T_{MAX} is the maximum transmittance upon applying an electric field and T_{OFF} is the transmittance after removing the applied electric field. One of the parameters used to evaluate the PDLC electro-optical response efficiency is the electric field required to achieve 90% of the maximum transmittance and is designated as E_{90}. The memory state contrast (MSC) is defined as the difference between T_{OFF} and T_0 and is reported as percentage.

However, PDLCs incorporating PEG6000 polymers exhibit an unexpected behavior, with 22% PME observed for PEG6000DA PDLCs and 13% for PEG6000DM PDLCs. This unexpected outcome may be attributed to the excessively long chain length, leading to a higher proportion of polymer chains in an amorphous phase. This amorphous arrangement enhances the PME compared to semi-crystalline PEG polymers with shorter chain lengths, such as PEG2000 and PEG4000.

4.3. Polarized Optical Micrographs

The structure of PDLC films was characterized using polarizing optical microscopy (POM). The images revealed that the PDLC films exhibited a uniform single-layer structure. The influence of longer chain lengths on crystalline morphology was evident, with typical spherulites observed, growing outward until they encountered neighboring spherulites [6] (see Figure 32j,l,n,p). In contrast, for smaller polymer chains (PEG2000 polymer), the crystalline shapes were smaller, leading to the absence of spherulitic morphology (see Figure 32f,h). Additionally, for the smallest polymer chain (PEG1000 polymer), a typical amorphous polymer structure was observed, wherein the liquid crystal was homogeneously dispersed within the polymer matrix. Interestingly, even in PDLC samples without PME, a residual alignment of liquid-crystal molecules persisted after the electric field was removed (see Figure 32f,h,j,l). However, this residual alignment was insufficient to achieve higher transparency, and a strong light-scattering state was reinstated, unlike the case of PEG1000 polymer/E7 PDLC, where a high transparency state was consistently maintained (see Figure 31a).

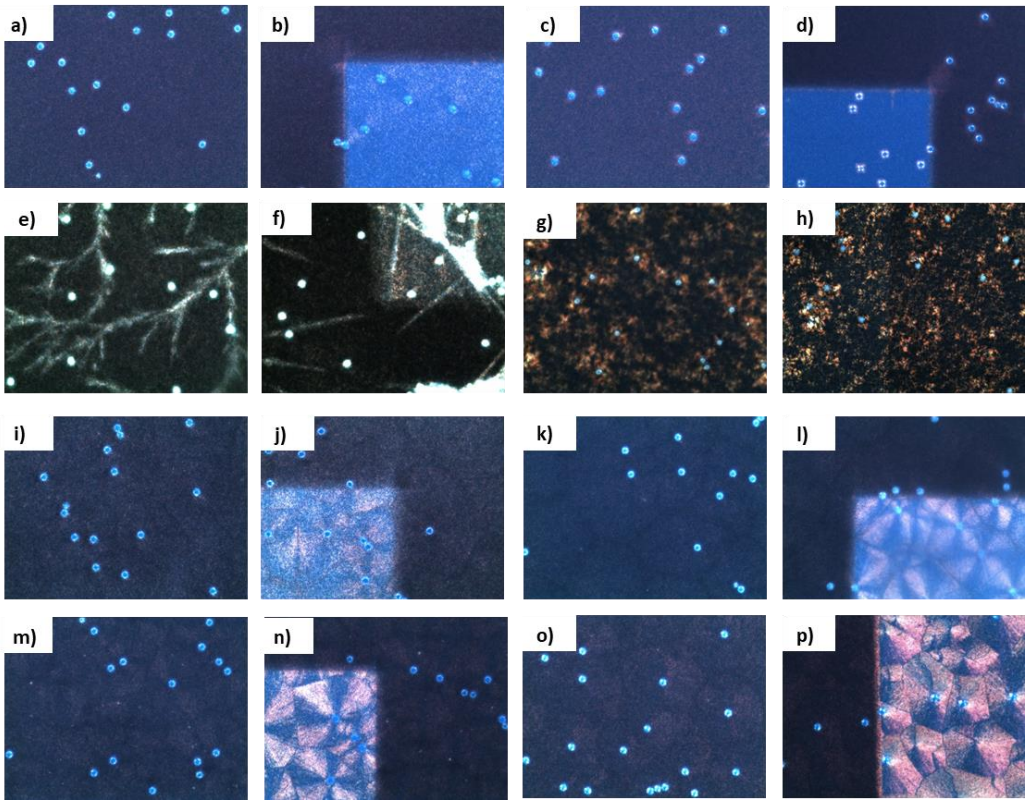

Figure 32. Polarized optical micrographs observed for PDLC samples: (**a**) initial OFF state of PEG1000DA PDLC; (**b**) OFF state upon removal of the applied electric field of PEG1000DA PDLC; (**c**) initial OFF state of PEG1000DM PDLC; (**d**) OFF state upon removal of the applied electric field of PEG1000DM PDLC; (**e**) initial OFF state of PEG2000DA PDLC; (**f**) OFF state upon removal of the applied electric field of PEG2000DA PDLC; (**g**) initial OFF state of PEG2000DM PDLC; (**h**) OFF state upon removal of the applied electric field of PEG2000DM PDLC; (**i**) initial OFF state of PEG4000DA PDLC; (**j**) OFF state upon removal of the applied electric field of PEG4000DA PDLC; (**k**) initial OFF state of PEG4000DM PDLC; (**l**) OFF state upon removal of the applied electric field of PEG4000DM PDLC; (**m**) initial OFF state of PEG6000DA PDLC; (**n**) OFF state upon removal of the applied electric field of PEG6000DA PDLC; (**o**) initial OFF state of PEG6000DM PDLC; (**p**) OFF state upon removal of the applied electric field of PEG6000DM PDLC, ×100 magnification.

4.4. Scanning Electron Microscopy

Figure 33 illustrates the morphology of the polymer matrix in the PEG PDLC. The morphology appears to be influenced by the degree of crystallinity of the polymer matrix. For both the smallest (PEG 1000 polymer) and the longest (PEG 6000 polymer) polymer chain lengths, a typical morphology resembling polymer balls is observed (see Figure 33a,b,g,h, respectively). In this morphology, the polymer forms agglomerates of polymer beads, creating an irregular network that facilitates a high degree of interconnection between the liquid-crystal (LC) domains. This morphology aligns with the permanent memory effect exhibited by these PDLC samples [23–25]. In contrast, for PEG2000 polymer (Figure 33c,d) and PEG4000 polymer (Figure 33e,f), a ring-shaped morphology is observed, possibly indicating an interfibrillar polymer structure that could be filled by the LC molecules.

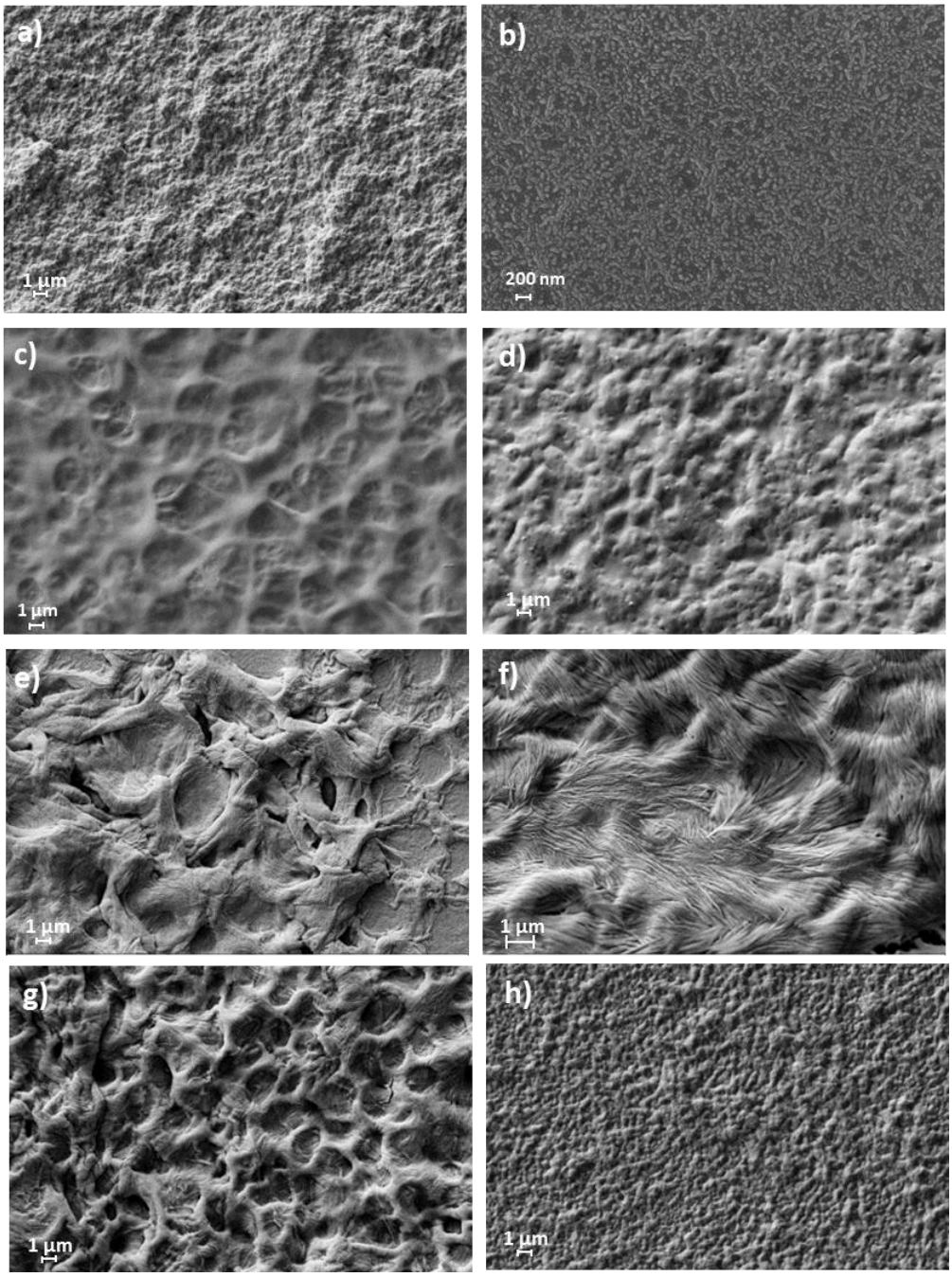

Figure 33. SEM micrographs for the microstructure of the polymer matrix of PDLC films prepared with different PEG pre-polymers: (**a**) PEG1000DA PDLC; (**b**) PEG1000DM PDLC; (**c**) PEG2000DA PDLC; (**d**) PEG2000DM PDLC; (**e**) PEG4000DA PDLC; (**f**) PEG4000DM PDLC; (**g**) PEG6000DA PDLC; and (**h**) PEG6000DM PDLC.

5. Conclusions

The molecular weight of linear polyethylene glycol pre-polymer, while maintaining two functionalities, significantly influences the thermal properties of the polymer, which in turn directly impacts the permanent memory effect (PME) of corresponding PDLC devices. Amorphous polymers like PEG1000DA with a glass transition temperature (Tg) at −48.46 °C and PEG1000DM with Tg at −45.30 °C promote a permanent memory effect of 43% and 31%, respectively. However, as the molecular weight increases, polymer chains become long enough to rearrange into a semi-crystalline structure, which negates the permanent memory effect of the corresponding PDLC. This correlation between the permanent memory effect

and the amorphousness/crystallinity of the polymer matrix could be attributed to the elasticity, flexibility, or stiffness of the polymer chains at the interface with LC molecules, which is in turn related to anchoring energy.

In PEG1000, the polymer chains are only long enough to interlink like cooked spaghetti, forming amorphous regions that provide enough ductility for the chain segments' structure to be affected by the LC alignment. Polymer chains existing at the interface between the polymer matrix and LC domains may reorient due to interactions with the reoriented LC molecules, altering the anchoring energy at the polymer/LC interface. This new anchoring energy maintains the LC director alignment when the electric field is switched off, leading to the permanent memory effect. However, as the molecular weight increases (PEG2000 and PEG4000), the polymer chain length becomes long enough to semi-crystallize, and the polymer chain segments become stiff enough to prevent LC alignment at the polymer/LC interface. The elastic force originating at this undistorted interface acts on the LC molecules in bulk to restore the random LC configuration of lower energy, resulting in a higher scattering state.

It is possible that longer polymer chains, such as PEG6000DA and PEG6000DM, crystallize with a larger proportion of chains in the amorphous phase, enhancing the PME to 22% and 13%, respectively.

Author Contributions: Synthesis and NMR characterization by A.M. and M.T.B.; PDLC preparation and electro-optical characterization by A.M. and J.S.; conceptualization by J.S.; writing—original draft preparation by A.M.; writing—review and editing by J.S.; supervision by J.S. All authors have read and agreed to the published version of the manuscript.

Funding: The NMR spectrometers are part of The National NMR Facility, supported by Fundação para a Ciência e a Tecnologia (RECI/BBB-BQB/0230/2012). This work was supported by the Associate Laboratory for Green Chemistry LAQV (UID/QUI/50006/2019) which is financed by national funds from FCT-MCTES and by FEDER funds through the COMPETE 2020 Program.

Data Availability Statement: The raw data supporting the conclusions of this article will be made available by the authors on request.

Conflicts of Interest: The authors declare no conflicts of interest.

References

1. Shao, L.; Zhang, Y.; Liu, C.; Li, J.; Qin, A.; Wang, Y. Effect of graft polymer prepared by living radical polymerisation on electro-optical properties of polymer dispersed liquid crystal. *Liq. Cryst.* **2012**, *39*, 1458–1464. [CrossRef]
2. Ravve, A. *Principles of Polymer Chemistry*; Springer: Berlin/Heidelberg, Germany, 2012.
3. Strobl, G. *The Physics of Polymers*; Springer: Berlin/Heidelberg, Germany, 2007.
4. Gedde, U.W. *Polymer Physics*; Springer: Berlin/Heidelberg, Germany, 2001.
5. Priola, A.; Gozzelino, G.; Ferrero, F.; Malucelli, G. Properties of polymeric films obtained from u.v. cured poly(ethylene glycol) diacrylates. *Polymer* **1993**, *34*, 3653–3657. [CrossRef]
6. Ward, I.M.; Sweeney, J. *An Introduction to the Mechanical Properties of Solid Polymers*; John Wiley & Sons, Ltd.: Hoboken, NJ, USA, 2004.
7. Pielichowski, K.; Flejtuch, K. Differential scanning calorimetry studies on poly(ethylene glycol) with different molecular weights for thermal energy storage materials. *Polym. Adv. Technol.* **2002**, *13*, 690–696. [CrossRef]
8. Godovsky, Y.K.; Slonimsky, G.L.; Garbar, N.M. Effect of molecular weight on the crystallization and morphology of poly(ethylene oxide) fractions. *J. Poymer Sci. C* **1972**, *21*, 1–21. [CrossRef]
9. Gao, W.; Bai, Y.; Chen, E.; Zhou, Q. Crystallization and melting of poly(ethylene oxide) confined in nanostructured particles with cross-linked shells of polybutadiene. *Chin. J. Polym. Sci.* **2005**, *23*, 275–285. [CrossRef]
10. Nishi, M.; Hikosaka, M.; Ghosh, S.K.; Toda, A.; Yamada, K. Molecular Weight Dependence of Primary Nucleation Rate of Polyethylene I. An Extended Chain Single Crystal. *Polym. J.* **1999**, *31*, 749–758. [CrossRef]
11. Bower, D.I. *An Introduction to Polymer Physics*; Cambridge University Press: Cambridge, UK, 2002.
12. Li, Y.; Ma, Q.; Huang, C.; Liu, G. Crystallization of Poly (ethylene glycol) in Poly (methyl methacrylate) Networks. *Mater. Sci.* **2013**, *19*, 147–151. [CrossRef]
13. Qiao, C.; Jiang, S.; Dong, D.; Ji, X.; An, L.; Jiang, B. The Critical Lowest Molecular Weight for PEG to Crystallize in Cross-Linked Networks. *Macromol. Rapid Commun.* **2004**, *25*, 659–663. [CrossRef]
14. Cheng, S.Z.D. *Phase Transitions in Polymers*; Elsevier: Amsterdam, The Netherlands, 2008.
15. Raju, G.G. *Dielectrics in Electric Fields*; Marcel Dekker, Inc.: New York, NY, USA, 2003.

16. Brás, A.R.E.; Henriques, S.; Casimiro, T.; Aguiar-Ricardo, A.; Sotomayor, J.; Caldeira, J.; Santos, C.; Dionísio, M. Characterization of a nematic mixture by reversed-phase HPLC and UV spectroscopy: An application to phase behaviour studies in liquid crystal-CO2 systems. *Liq. Cryst.* **2007**, *34*, 591–597. [CrossRef]
17. Zhang, B.; Zhang, H.; Myers, B.K.; Elupula, R.; Jayawickramarajah, J.; Grayson, S.M. Determination of polyethylene glycol end group functionalities by combination of selective reactions and characterization by matrix assisted laser desorption/ionization time-of-flight mass spectrometry. *Anal. Chim. Acta* **2014**, *816*, 28–40. [CrossRef] [PubMed]
18. Yu, D.; Vladimirov, N.; Fréchet, J.M.J. MALDI-TOF in the Characterizations of Dendritic−Linear Block Copolymers and Stars. *Macromolecules* **1999**, *32*, 5186–5192. [CrossRef]
19. Lin-Gibson, S.; Bencherif, S.; Cooper, J.A.; Wetzel, S.J.; Antonucci, J.M.; Vogel, B.M.; Horkay, F.; Washburn, N.R. Synthesis and characterization of PEG dimethacrylates and their hydrogels. *Biomacromolecules* **2004**, *5*, 1280–1287. [CrossRef] [PubMed]
20. Casey, B.K.; Lapucha, J.E.; Grayson, S.M.; Myers, B.K.; Lapucha, J.E.; Grayson, S.M. Synthesis and MALDI-ToF characterization of dendronized poly(ethylene glycol)s. *Braz. J. Pharm. Sci.* **2012**, *49*, 45–55.
21. Ginés, J.M.; Arias, M.J.; Rabasco, A.M.; Novák, C. Thermal characterization of polyethylene glycols applied in the pharmaceutical technology using differential scanning calorimetry and hot stage microscopy. *J. Therm. Anal.* **1996**, *46*, 291–304. [CrossRef]
22. Craig, D.Q.M.; Newton, J.M. Characterisation of polyethylene glycols using differential scanning calorimetry. *Int. J. Pharm.* **1991**, *74*, 33–41. [CrossRef]
23. Santos, R.; Silva, M.C.; Mouquinho, A.; Sotomayor, J. Full permanent memory effects in PDLC films. *Mol. Cryst. Liq. Cryst.* **2015**, *611*, 123–131. [CrossRef]
24. Mouquinho, A.; Luís, N.; Sotomayor, J. New polymer to enhance the permanent memory effect of polymer-dispersed liquid crystals films. *J. Appl. Polym. Sci.* **2016**, *133*, 43482. [CrossRef]
25. Drzaic, P.S. *Liquid Crystal Dispersions*; Ong, H.L., Ed.; World Scientific Publishing: Singapore, 1995.